

1 **Peat humification records from Restionaceae bogs in northern New**
2 **Zealand as potential indicators of Holocene precipitation, seasonality,**
3 **and ENSO**

4
5 Rewi M. Newnham¹, Zoë J. Hazell^{2*}, Dan J. Charman³, David J. Lowe⁴, Andrew B.H.
6 Rees¹, Matthew J. Amesbury^{3,5}, Tom P. Roland³, Maria Gehrels⁶, Valerie van den
7 Bos¹, Ignacio A. Jara⁷

8
9 ¹ *School of Geography, Environment & Earth Sciences, Victoria University of*
10 *Wellington, PO Box 600 Wellington, New Zealand*

11 ² *Historic England, Fort Cumberland, Fort Cumberland Road, Eastney, Portsmouth,*
12 *Hampshire, PO4 9LD, UK.*

13 ³ *Geography, College of Life and Environmental Sciences, University of Exeter,*
14 *Exeter, UK*

15 ⁴ *School of Science, University of Waikato, Private Bag 3105, Hamilton, 3240, New*
16 *Zealand*

17 ⁵ *Environmental Change Research Unit (ECRU), Faculty of Biological and*
18 *Environmental Sciences, University of Helsinki, Finland*

19 ⁶ *Environment Department, York University, United Kingdom*

20 ⁷ *Centro de Estudios Avanzados en Zonas Áridas (CEAZA), Colina del Pino, La*
21 *Serena, Chile*

22
23 **corresponding author: rewi.newnham@vuw.ac.nz*
24

25 **ABSTRACT**

26 In comparison with temperature reconstructions, New Zealand proxy records for
27 paleo-precipitation are rare, despite the importance of precipitation in contemporary
28 climate variability and for projected climate impacts. In this study, records of mid-late
29 Holocene palaeomoisture variation were derived for two hydrologically separate
30 ombrotrophic Restionaceae bogs in northern New Zealand, based on peat
31 humification analysis. At each site, three cores were analysed for peat humification,
32 facilitating both intra- and inter-site comparisons. Age models for the six sequences
33 were developed using radiocarbon dating and tephrochronology. Twelve tephras
34 (including six cryptotephras) were recognised, four of which were used to precisely
35 link the two sites and to define start and end points for the records at 7027 ± 170
36 (Tuhua tephra) and 1718 ± 10 cal. yr BP (Taupo tephra) (2σ -age ranges), respectively.
37 We find individual differences between the six peat humification records at short-term
38 timescales that are presumably due to local site factors, in particular changing
39 vegetation and microtopography, or to changes in the composition of the material
40 analysed. Stronger longer-term coherence is observed between all six records but is
41 attributed to slow anaerobic decay over time because the implied trend towards wetter

42 summers in the late Holocene cannot be corroborated by independent climate proxies.
43 Despite these confounding factors, centennial scale shifts in bog surface wetness are a
44 pervasive feature of all six records with varying degrees of overlap in time that show
45 strong correspondence with El Niño-Southern Oscillation reconstructions from the
46 eastern equatorial Pacific. These results indicate the potential for peat humification
47 records from New Zealand's ombrotrophic bogs to elucidate past climate variability
48 and also demonstrate the importance of developing multiple well-dated profiles from
49 more than one site.

50

51 **KEYWORDS:** peat humification, ENSO, tephrochronology, effective precipitation,
52 Bayesian age modelling

53

54 **1.0 Introduction**

55

56 During the past few decades, changes to the hydrological cycle and precipitation
57 patterns across the planet have been linked to short-term (annual to decadal)
58 variability in regional climate modes (e.g., Wang & Cai, 2013; Hartmann et al., 2013).
59 In extratropical regions of the Southern Hemisphere such as New Zealand, these
60 patterns, in large part, are explained by a shift towards the high-index positive phase
61 of the Southern Annular Mode (SAM; Marshall, 2003; Renwick, 2005; Kidston et al.,
62 2009) and in northern New Zealand by stronger or more frequent El Niño events as
63 part of more variable ENSO cycles (Salinger & Mullan, 1999; Ummenhofer &
64 England, 2007; Gergis & Fowler, 2009). The recent trend in the SAM has been linked
65 both to increases in greenhouse gases and stratospheric ozone depletion (Fogt et al.,
66 2009; Thompson et al., 2011) and may be unprecedented in the last millennium at
67 least (Abram et al., 2014; Jones et al., 2016). However, as the observational record
68 extends for just a few decades, there is an important need to set these projections and
69 the recent observed trend into a longer historical context. As precipitation variability
70 is a primary indicator for both SAM and ENSO in the southern extratropics (Garreaud
71 et al., 2007), the key to reconstructing past variability in these climate modes lies with
72 finding suitable localities, depositional environments, and proxies to reconstruct
73 paleoprecipitation.

74

75 New Zealand is well-served in the first two of these three requirements, but with the
76 notable exception of hydroclimate inferences drawn from speleothem stable isotope
77 records (e.g., Williams et al., 2004), there have been only a few attempts to develop
78 other precipitation proxies. Here we explore the potential of peat humification
79 analysis applied at two raised bogs in northern New Zealand for reconstructing past
80 effective precipitation (precipitation minus evapotranspiration). The method has been
81 widely applied in other regions of the world, although some questions have been
82 raised about its suitability as a paleo-precipitation proxy (see section 2.0). Yet to date
83 only two humification studies have been reported from New Zealand, both from sites
84 in the southern South Island (McGlone & Wilmshurst, 1999; Wilmshurst et al., 2002).
85 Nevertheless, there appears to be good potential in this oceanic setting characterised
86 by strong regional differentiation of hydroclimate and an abundance of raised
87 ombrotrophic (rain-fed) bog sites.

88

89 We present multiple humification records, linked precisely via tephrochronology and
90 dated using multiple AMS and conventional radiocarbon (^{14}C) ages, from two
91 hydrologically separate ombrotrophic bogs in northern New Zealand, that span the
92 interval ca 7.0–1.7 calendar/calibrated (cal) ka (all ages calibrated in this study are
93 referred to as cal years BP or cal ka). We test the feasibility of northern New Zealand
94 humification records for reconstructing past precipitation at two time scales for the
95 Holocene: (1) decadal-centennial and (2) millennial scales. Within- and between-site
96 replicability and comparison with other paleo-climate records provide a basis for
97 evaluation: coherent humification patterns within and between the two sites and with
98 other records would support the conclusion that they represent regional precipitation
99 patterns.

100

101 **2.0 Peat humification as a paleoclimate proxy: potential and limitations**

102

103 Humification of peat deposits is a widely used paleoclimate proxy that extends back
104 to the 19th century in northern Europe (; Zaccone et al., 2018). The modern era of
105 climate reconstruction from peat bogs follows the principle that raised mires in
106 particular could provide continuous records of past hydroclimatic change because
107 they are directly coupled with the atmosphere (Aaby & Tauber, 1975; Barber, 1981).
108 The underlying premise is that peat humification is a measure of organic decay that

109 mainly reflects changing paleohydrological conditions in the thin upper layer or
110 acrotelm. This layer experiences seasonal water table fluctuations, determined largely
111 by the balance between precipitation and evapotranspiration, with associated
112 variability in rates of decomposition. In contrast, decomposition proceeds much more
113 slowly in the anaerobic catotelm and so the degree of peat humification is thought to
114 represent the environmental conditions and in particular bog surface wetness (BSW)
115 at the time of peat accumulation (Aaby & Tauber, 1975; Blackford & Chambers,
116 1993). Building on this important premise, a suite of climate proxies has been
117 developed and applied to Late Quaternary peat archives.

118

119 Although there is a sound conceptual basis, questions have been raised about the
120 wider applicability of humification as a paleoclimate proxy (Chambers et al, 2012;
121 Hughes et al., 2012; Zaccone et al., 2018), such questions being supported by studies
122 that reported inconsistencies between humification and other proxy-records of surface
123 wetness in a peat profile (Yeloff & Mauquoy, 2006; Amesbury et al., 2012). One
124 likely issue is that past changes in botanical composition at the core site may have an
125 influence on humification measurements (Chambers et al., 1997; Payne & Blackford,
126 2008; Hughes et al., 2012). This issue may be compounded by the small sample sized
127 used for measurement. Others have suggested that local topography and geochemical
128 characteristics of the peat may also influence humification values, while some work
129 has questioned the reliability of the colorometric technique itself for determining
130 humification values (Caseldine et al., 2000; Morgan et al., 2005). Amesbury et al.
131 (2012) also challenged the use of composite curves of BSW that combined results
132 from multi-proxy studies. They showed that climate proxies derived from analyses of
133 testate amoebae, plant macrofossils, and peat humification at an ombrotrophic bog
134 from western Sweden were correlated with climate parameters but at different time
135 scales, suggesting that climate-proxy response times and regional variability may be
136 greater than previously hypothesised. In another study from Sweden that used a
137 similar approach to ours, Borgmark & Wastegård (2008) analysed five peat
138 humification records from three ombrotrophic bogs in order to reduce the influence of
139 local fluctuations and extract regional climate signal.

140

141 Historically, peatland proxy-climate research has been undertaken mostly in northern
142 Europe, but is becoming more prominent in parts of Asia and North America. In New

143 Zealand, a long history of peatland research extends back to the seminal work of
144 Cranwell and von Post (1936) and has perhaps gained less international recognition
145 than in other areas (the reader is referred to McGlone, 2009, for an account of New
146 Zealand Holocene peat records; see also Davoren, 1978). Nevertheless, climate
147 reconstructions from New Zealand peatlands are being applied increasingly to
148 elucidate hemispheric and global patterns and test postulated climate forcing
149 mechanisms (e.g., Newnham et al., 2012; Turney et al., 2017). The New Zealand
150 work has mostly deployed pollen analysis, sometimes combined with plant
151 macrofossil analysis (e.g., Newnham et al., 1993; 1995a; Ogden et al., 1993; McGlone
152 & Wilmshurst, 1999; Haenfling et al., 2015; Jara et al., 2017), stable isotopes of plant
153 macrofossils (McGlone et al., 2004), or testate amoebae (Wilmshurst et al., 2002).
154 Recent investigations of the stable isotopic composition of New Zealand Restionaceae
155 peat across modern climate gradients also indicate strong potential for these proxies in
156 climate reconstruction (Amesbury et al., 2015a and b). In northern New Zealand,
157 considerable effort has been applied to developing tephrostratigraphic records from
158 peat profiles, both to provide a robust chronostratigraphic framework for correlating
159 sites, for independently dating climate reconstructions, and to help evaluate volcanic
160 history and risk (Lowe et al., 1999, 2008, 2013; Alloway et al., 2004; Gehrels et al.,
161 2006; Newnham et al., 1995a, 1995b; Newnham et al., 1999). Tephrostratigraphy
162 provides a key chronstratigraphical tool in the current study.

163

164 **3.0 Study sites and regional setting**

165

166 Two raised, ombrotrophic bogs, ca 55 km apart in the Waikato region, were
167 investigated (Fig. 1). At Kopuatai and Moanatuatua bogs, thick sequences of peat
168 have accumulated on the surface of volcanoclastic alluvial deposits (Hinuera
169 Formation) of the river systems that drained the central North Island volcanic plateau
170 during the last glacial (Selby and Lowe, 1992; Manville and Wilson, 2004; Edbrooke,
171 2001, 2005). The peat profiles at the two sites span much the same timeframe, and
172 contain similar suites of tephra layers that enable correlation between sequences and
173 help test and constrain ^{14}C age models developed for them. Cored peat deposits
174 extracted from the bogs have been described in a number of earlier studies (de Lange
175 and Lowe 1990; Hodder et al., 1991; Newnham et al., 1995a; Shearer, 1997; Gehrels
176 et al., 2006; Haenfling et al., 2015; Jara et al., 2017) and are summarised in Fig. 2.

177 *Fig 1 here

178 *Fig 2 here

179 The vegetation communities growing at both bogs show low plant diversity with only
180 10–15 common species. Most prominent are two species of the Southern Hemisphere
181 Restionaceae (or restiad) family: *Empodisma robustum* (lesser wire rush) and
182 *Sporadanthus ferrugineus* (greater wire rush or cane rush) (de Lange *et al.*, 1999;
183 Wagstaff and Clarkson, 2012), while other common species include *Leptospermum*
184 *scoparium* (Myrtaceae), the fern *Gleichenia dicarpa*, epacrids *Dracophyllum*
185 *scoparium* and *Epacris pauciflora*, and several sedges in the genera *Schoenus* and
186 *Baumea*. Sundews (*Drosera*) may be locally common along with *Sphagnum*
187 *cristatum*. The two restiad species, and in particular *Empodisma*, are the main peat
188 formers and have an essential role in the development of bog environments in this
189 region. Their extensive surface-growing rhizome systems and extremely low
190 evapotranspiration rates enable far greater water retention in a region that experiences
191 frequent summer moisture deficits and therefore is not otherwise considered
192 conducive to peat development (Campbell and Williamson, 1997; Kuder *et al.*, 1998;
193 Thompson *et al.*, 1999; Campbell and Jackson, 2004; Ratcliffe *et al.*, 2019). The
194 detailed vegetation composition and structure of these bogs were described by
195 Clarkson (2002), Clarkson *et al.* (2004), and Wagstaff and Clarkson (2012).

196

197 Climate of the Waikato region is classed as warm temperate and fully humid (class
198 Cfb as defined in Kottke *et al.*, 2006). In recent decades, annual precipitation has
199 ranged between 1112 and 1500 mm and annual mean temperatures between 13.0 and
200 14.3 °C in lowland regions (Clarkson *et al.*, 2004). Precipitation is stronger in winter
201 (July, ~126 mm) than in summer (February, ~71 mm), and monthly rainfall minima
202 often coincide with the two warmest months, January and February (NIWA, 2009).
203 As a consequence, summer moisture deficits are common at these bogs and typical
204 annual water deficits exceed ~60 mm (Clarkson *et al.*, 2004; Amesbury *et al.*,
205 2015a&b; Goodrich *et al.*, 2017). Weather conditions (mean air temperature, annual
206 rainfall) across the two sites are broadly similar (Ratcliffe *et al.*, 2019).

207

208 **3.1. Kopuatai** (centre: 37°26'S, 175°34'E)

209 Kopuatai Bog is an internationally-recognised wetland (Ramsar Site 444) and the
210 largest remaining natural-state peat bog in New Zealand at 18 km long and 10 km
211 wide (Maggs, 1997). It is situated 2–6.5 m above sea level in the Hauraki Depression,
212 a 20-30 km wide rift in the Hauraki lowlands (de Lange & Lowe, 1990; Persaud et al.,
213 2016). Its raised centre is 3 m above the surrounding edges and the maximum peat
214 depth is 12–14 m in central areas (Davoren, 1978; Newnham et al., 1995a). Around ca
215 7400 cal years BP the northern end of the site was flooded by a marine transgression,
216 directly depositing a thick deltaic mud in the flooded areas and indirectly resulting in
217 the deposition of a minerogenic, freshwater deposit associated with local ponding in
218 the northern area (Newnham et al., 1995a). Two such mud layers were recorded in
219 cores K106 and K204 (Fig. 2). The evolution of the bog and its Holocene vegetation
220 history have been reported previously from pollen, plant macrofossil, and charcoal
221 records (Newnham et al., 1995a).

222

223 **3.2. Moanatuatua** (centre: 37°58'S, 175°72'E)

224 Situated ~55 km inland and southwest of Kopuatai, Moanatuatua bog was once of
225 similar size, but extensive agricultural drainage schemes since the 1930s have reduced
226 its extent to just 1.1 km² (Cranwell, 1939; Clarkson et al., 1999; Thompson *et al.*,
227 1999; Clarkson, 2002; Pronger et al., 2014). The remaining bog, protected as a
228 scientific reserve, is 65 m above sea level, with a peat dome 1–2 m above the
229 surrounding farmland and peat depths reaching 13 m. In the surrounding pasture,
230 farming practices have removed the top 1–2 m of sediment from the edges of the
231 peatland, as demonstrated by the comparison of depths of tephra layers from within
232 and outside the reserve (Shearer, 1997; Schipper and McLeod, 2002). The Holocene
233 vegetation history of Moanatuatua Bog has been shown previously from pollen (Jara
234 et al., 2017) and plant cuticle (Haenfling et al., 2015) records.

235

236 **4.0 Material and methods**

237

238 **4.1. Fieldwork**

239

240 At each site, three cores were collected within 300–500 m of one another (Fig. 1) to
241 test replicability between sequences and to develop composite records from multiple
242 cores. Sampling was guided by two prominent tephra layers that were visible in all

243 core sequences (Fig. 2): Tuhua Tephra, c. 7.0 cal ka (Lowe et al., 2013), and Taupo
244 Tephra, c. 1.7 cal ka (Hogg et al., 2012). The humification analyses were confined to
245 the peats in this interval because, below the Tuhua Tephra, marine influence on the
246 Kopuatai hydrology could not be discounted and the near-surface post-Taupo
247 sediments proved in some cases to be too sloppy or fibrous to sample intact. Two
248 other marker tephras were common to both bogs hence further enabling core
249 correlation: Mamaku Tephra, c. 8.0 cal ka and Whakaipo Tephra, c. 2.8 cal ka (see
250 chronology section below). All but one core location were from protected areas,
251 sufficiently far from the drained margins to avoid the likely impacts on peat
252 composition and hydrology (Fig. 1). The exception, core M102, sampled from
253 pastureland adjacent to the Moanatuatua reserve, has a very similar pre-Taupo tephra
254 record to that of the other two cores from this site and so the sediments analysed in
255 this study are unlikely to have been affected by the land use modifications of the past
256 few decades.

257

258 All cores were extracted using “Russian”-type D-shaped corers. Core sections were
259 extracted in alternate, overlapping sections from two holes *c.* 1 m apart to avoid gaps
260 and to prevent disturbance of the adjacent, lower-lying sediment by the corer’s
261 pointed nose. Once retrieved, all cores were stored in plastic piping, wrapped in non-
262 PVC clingfilm, and refrigerated at 4°C.

263

264

265 **4.2 Laboratory analyses**

266

267 **4.2.1 Core subsampling**

268

269 The uppermost subsample from each core was taken from the 1 cm section
270 immediately below the Taupo Tephra layer, with subsequent samples extracted down-
271 core at regular intervals. For humification, water content, and total organic carbon
272 analyses, one core from each site (Kopuatai K204 and Moanatuatua M206) was
273 sampled every 2 cm, which represents an estimated between-sample time interval of
274 20 to 40 years. The other two cores at each site were sampled every 4 cm. Each sub-
275 sample was 1-cm thick due to the fibrous nature of the peat preventing finer-
276 resolution subsampling. A suite of analyses was carried out on each sample as
277 described below.

278

279 **4.2.2 Total organic carbon**

280

281 Samples were oven-dried overnight then water content was calculated as a percentage
282 of the total wet weight. Total organic carbon (TOC) was measured using a Shimadzu
283 TOC5000 TOC analyser, with the solid sample module-5000A furnace at 900°C. This
284 method was used in preference to loss-on-ignition because of the small amount of
285 sample required for processing. For each sample, three repeat measurements were
286 taken, and averaged. The results were used to correct for mineral content within peat
287 samples, to determine a cut-off point for inclusion in humification analyses as
288 described below, and to assist in determining the positions of cryptotephra deposits in
289 these sequences (Gehrels et al., 2006).

290

291 **4.2.3 Humification**

292 Peat humification was determined using the colorimetric method based on the light
293 transmission of the alkali-extracted humic acids in solution (Blackford and Chambers,
294 1993). Light transmission is inversely related to the degree of peat decomposition: the
295 more decomposed or humified the sample, the less light transmitted. The degree of
296 peat humification is largely controlled by moisture level of the near-surface peats,
297 which in ombrotrophic bogs is determined by effective precipitation. Thus light
298 transmission can be used as a proxy for ‘bog wetness’ reflecting the balance of
299 precipitation and evaporation. In this study, following the method of Blackford and
300 Chambers (1993), percentage light transmission was measured at a wavelength of 550
301 nm on a Zeiss Specord M500 spectrophotometer. For each sample, three readings
302 were taken and the mean value calculated.

303

304 *Correction for minerogenic content*

305 The relationship between light transmission and peat humification can be distorted in
306 peat samples containing minerogenic constituents, which may be comparatively high
307 in the Waikato peats because of volcanogenic (tephra-fall derived) matter. The
308 presence of some highly minerogenic (tephra, clay) samples made it necessary to
309 determine a cut-off point beyond which light transmission values could not be used
310 confidently to reflect peat humification. In this study, light transmission data for
311 samples with <45% TOC were ignored as these samples corresponded with visible

312 tephra or clay layers. For the remaining (peat-rich) samples with >45% TOC, it was
313 necessary to correct light transmission values for any distortion caused by varying
314 levels of minerogenic matter. Previous work recommended a simple linear correction
315 for this effect based on the minerogenic content determined by LOI (Blackford and
316 Chambers, 1993; Roos-Barraclough et al. 2004; Chambers et al., 2011). Hazell (2004)
317 developed a modified procedure after finding a non-linear relationship between
318 mineral content and light transmission in these Waikato peats. In this study we use the
319 procedure developed by Hazell (2004) to correct for mineral matter based on this non-
320 linear relationship (see Supplementary Information for details).

321

322 *Detrending for long-term decay effect*

323 Because humification proceeds incrementally with time, it is necessary to consider the
324 possibility that the corrected humification measurements may in part reflect the
325 effects of long-term decay (Clymo, 1984). To counter this possible effect, some
326 workers (e.g., Borgmark and Wastegård, 2008) have presented humification data as
327 normalised and detrended, usually by linear regression with the assumption that long-
328 term anaerobic decay of peat occurs linearly over time. This approach is valid when
329 the goal is solely to investigate shorter term climate ‘shifts’ but it precludes the
330 possibility of investigating longer term shifts in climate. To allow for this possibility
331 as well, our approach was to present the humification values in both detrended and
332 non-detrended form. We use the detrended data to investigate shorter term climate
333 shifts and the raw corrected (non-detrended) data to consider the possibility of longer
334 term climate trends. We then compare these longer term humification trends with
335 independent climate proxy records from these sites and elsewhere in the region to
336 evaluate whether long-term decay or climate is the more likely controlling factor.

337

338 To detrend the data, simple linear regression by age was applied to each humification
339 record and residuals from the regression line were calculated. Both detrended
340 residuals and raw data were normalised to the period between the Tuhua and Taupo
341 tephra (c 7000-1700 cal. yr BP), a period common to all cores.

342

343 *Correlation of humification records at decadal-centennial scale*

344

345 We conducted correlation analysis to test for the coherence between the three
346 humification records developed at each site. Using the age models developed, we
347 divided each sequence into 100-year bins and calculated the mean humification value
348 for each bin. We then calculated the Pearson product moment correlation coefficients
349 between each pair of sequences. The associated P values enabled a test of significance
350 for each correlation.

351

352 **4.3 Chronology**

353

354 The cores comprised mainly peat with sparse occurrences of small plant macrofossils
355 (or fragments of such material), occasional visible tephra layers each between a few
356 millimetres or centimetres in thickness, and a 30–50 cm clay layer in two cores from
357 Kopuatai (Fig. 2). A combination of tephrochronology and radiocarbon dating was
358 used to derive detailed age-depth models and to correlate cores within and between
359 sites.

360

361 **4.3.1 Stratigraphy and chronology of tephras**

362

363 Twelve tephras in total were identified, six as visible layers, five as cryptotephras
364 (glass shard and/or crystal concentrations insufficiently numerous, or too fine, to be
365 visible as a layer to the naked eye: Lowe, 2011), and one (Whakaipo) as a thin layer in
366 one core but as a cryptotephra deposit in others (Fig. 2). All but two of the tephras are
367 rhyolitic in composition and were able to be correlated with characterised and defined
368 equivalent deposits elsewhere; two are andesitic and remain uncorrelated but their
369 compositions indicate that they were derived from Egmont volcano (Fig. 1; Table 1).
370 The tephras were correlated using a combination of stratigraphic position, field
371 properties, ferromagnesian mineralogical assemblages (Lowe, 1988; Hodder et al.,
372 1991; Newnham et al., 1995a), and new major element analyses of volcanic glass
373 shards as reported below.

374 **Table 1 here*

375

376 Glass-shard major element compositions were obtained for nine samples from
377 Kopuatai and eight samples from Moanatuatua (Tables 2 and 3, respectively) using a
378 Jeol-JXA ‘Superprobe’ electron microprobe housed at the Analytical Facility,

379 Victoria University of Wellington. The Kopuatai analyses were supplemented by
380 previously-reported analyses on four cryptotephra and on Kaharoa Tephra (Table 2).

381 **Tables 2&3 here*

382

383 **4.3.2 Radiocarbon dating**

384 Fifty-five radiocarbon ages were obtained from the two sites (Fig. 2; Table 4). Of
385 these, seven were radiometric dates on bulk peat samples, processed at the Waikato
386 Radiocarbon Dating Laboratory, University of Waikato, Hamilton, New Zealand.

387 These dated specific stratigraphic layers (base of sequence, tephra layers, and the clay
388 layer in Kopuatai cores K106 and K204) and confirmed the preliminary field-based
389 tephra identifications. Two of these bulk ages were taken from nearby cores not used
390 in this study but are included here for completeness (Table 4).

391 **Table 4 here*

392

393 The remaining forty-eight ages were determined by accelerator mass spectrometry
394 (AMS) on above-ground plant macrofossils, processed at the NERC Radiocarbon
395 Laboratory, East Kilbride, UK. These were spaced between the already well-dated
396 Tuhua and Taupo tephra layers. Macrofossils used for dating were mainly
397 *Leptospermum scoparium* and *Epacris pauciflora* leaves as these were generally
398 common and well-preserved or, where these were absent or infrequent, *Epacris* and cf.
399 *Empodisma* seeds, and *Gleichenia dicarpa* fronds.

400

401 **4.3.3 Age-depth models**

402

403 **Figure 3 here*

404

405 The age-depth models presented here (Fig. 3) were developed using the SHCal13
406 atmospheric curve (Hogg et al., 2013) in OxCal v4.3.2 (Bronk Ramsey, 2017). Both
407 the 55 radiocarbon dates (Table 4) and preferred Lowe et al. (2013) ages for nine
408 tephra (Table 1) were modelled using P_Sequence commands (Bronk Ramsey, 2008)
409 for each of the six cores; outliers were analysed with the General model (Bronk
410 Ramsey, 2009). Running the P_Sequence models together permits cross-referencing
411 tephra between cores, treating these deposits as coeval isochrons.

412

413 **5 Results**

414

415 5.1. Kopuatai

416 The three Kopuatai cores comprise dark brown peat throughout, interbedded with
417 millimetre-to-centimetre scale visible tephra layers. As noted earlier, two of the
418 Kopuatai cores include a minerogenic layer dated to c. 7400–6900 cal yr BP and
419 thereafter transitioning upwards into peat. As the light transmission properties of clay
420 are distinctly different to those of peat, humification results are not presented for the
421 clay layer and we restrict our comparisons of humification records to the period
422 6500—1700 cal yr BP, when peat formation is dominant at all six core sites.

423

424 In all three sequences, moisture content and TOC remain consistent at 90–95% and c.
425 60%, respectively, except around tephra layers. Marked oscillations are evident in the
426 light transmission values which vary between 10–30% away from prominent tephra
427 layers.

428

429 The light transmission curves for the three sequences are compared against a common
430 timescale in Figure 4a. All three records show similar short-term oscillations
431 superimposed on a long-term trend towards increasing light transmission (reduced
432 humification) commencing between 5000 and 4000 cal yr BP.

433

434 **Figure 4 here*

435

436 In Figure 5a, the 100-year averages for the three detrended Kopuatai humification
437 records are able to be compared. They display coherent intervals where all three
438 records gave the same trend (positive or negative humification trends). Consistently
439 wetter intervals are indicated for 3800–3300 cal yr BP and for 2000–1700 cal yr BP
440 whereas the period 2400–2000 is mostly wetter than average. Consistently dry
441 conditions are indicated for the interval 4900–4300 cal yr BP and the period 3300–
442 2400 is mostly drier than average. Outside of these intervals, there is no coherent
443 pattern indicated across the three records.

444

445 **Fig 5 here*

446 Correlation analysis indicates a significantly ($p < 0.05$) positive relationship overall
447 between the 100-year humification averages for K204 and the other two core records,
448 but not between K106 and K108 (Table 5).

449

450 **Table 5 here*

451 **5.3 Moanatuatua**

452

453 The three Moanatuatua cores, similar to the Kopuatai cores, comprise dark brown peat
454 throughout, interbedded with millimetre-to-centimetre scale visible tephra layers as
455 well as cryptotephra glass concentrations (Fig. SI2). In all three sequences, moisture
456 content and TOC remain consistent at 85–90 % and *c.* 50 %, respectively, except
457 around tephra layers. As for the Kopuatai cores, marked oscillations are evident in the
458 light transmission values which range from 10–25 %.

459

460 The corrected light transmission curves for the three sequences are compared against
461 a common timescale in Figure 4b. As at Kopuatai, there is a consistent long-term
462 trend towards increasing light transmission values after *c.* 4500 cal yr BP.

463

464 Comparison of the three detrended Moanatuatua humification records in 100-year
465 bins (Fig. 5b) shows mostly wetter intervals for 7000–6400 cal yr BP, 4600–4200 cal
466 yr BP, 3600–3400 cal yr BP, 2900–2500 cal yr BP, and 2100–1700 cal yr BP. The
467 intervals 5500–4600 cal yr BP and 4200–3700 cal yr BP are mostly dry and 2500–
468 2100 cal yr BP is consistently dry for all three records. Outside of these intervals,
469 there is no coherent pattern indicated across the three records.

470

471 Correlation analysis indicates a significantly ($p < 0.05$) positive relationship between
472 the 100-year humification averages for M103 and M102 only with the other two core
473 pairs not significantly correlated with one another (Table 5).

474

475 **6 Discussion**

476 **6.1 Interpretation of peat humification records**

477 Light transmission indicates the overall degree of peat humification for the estimated
478 *c.* 20–40 year time period encapsulated by each sample. Large changes in
479 humification should be predominantly representative of the average aeration at the
480 bog surface during this interval, which in ombrotrophic bogs is a function of the
481 balance between precipitation and evapotranspiration (P-E). Under normal conditions

482 of a high and stable water table, seen today at Kopuatai and prior to drainage at
483 Moanatuatua (Ratcliffe et al., 2019), bog surface wetness and hence P-E balance vary
484 markedly through the seasonal cycle (Maggs, 1997; Fritz et al., 2008; Ratcliffe et al.,
485 2019). During winter, the water table typically reaches a maximum and excess
486 precipitation may be lost as runoff – during this time the water table rarely drops
487 below a threshold that permits aerobic decay in the surface peat. The main period of
488 peat decay is therefore the summer season when the near-surface peat is subject to
489 biologically important changes in moisture and aeration and also to the highest
490 temperatures. In Northern Hemisphere temperate peatlands, warm-season moisture
491 deficit has been shown to be the main driver of decadal-scale changes in water table
492 (Charman, 2007; Charman et al., 2009) and it seems likely that a similar relationship
493 exists in New Zealand restiad peatlands. However, temperature can also be a direct
494 driver of humification, independent of evaporation, through stimulation of microbial
495 activity. In a number of bogs with very deep water tables, water table fluctuation can
496 have little effect on peat surface moisture content, and thus decay, with humification
497 almost entirely driven directly by temperature, rather than P-E and water table. This is
498 the case in a number of un-modified bogs (Lafleur et al., 2005; Euskirchen et al.,
499 2014) and in Moanatuatua post-drainage (Ratcliffe et al., 2019). However, we would
500 anticipate that any disconnect between water table and humification would be
501 accompanied by a sustained shift towards high humification, itself indicative of a low
502 frequency change in P-E. We are thus cautious about attributing high-frequency
503 changes in humification to P-E in the more humified sections of the core but consider
504 that the downcore variations in peat humification will generally reflect the combined
505 effects of summer precipitation and temperature variability. ‘Summer’ in this context
506 may actually be defined as an extended summer season covering all the months in
507 moisture deficit rather than simply a notional December to February period (Charman
508 et al., 2009).

509

510 **6.2. Millennial-scale inferred moisture variability**

511 The sampling strategy and analyses deployed here were designed to allow for the
512 possibility of climate forcing of long-term (millennial scale) humification values by
513 examining raw corrected light transmission values at this scale. As stated earlier, light
514 transmission is inversely related to the degree of peat decomposition so the more

515 decomposed or humified the sample, the less light transmitted. The underlying
516 premise is that replicated patterns in humification between and within sites are more
517 likely to represent regional climate signals.

518

519 The most striking pattern evident in all records at both sites is that corrected light
520 transmission values show an increasing positive trend, indicating decreasing
521 humification overall after c. 4000 cal yr BP, albeit with strong variability. Because the
522 same long-term trends, well-constrained chronostratigraphically, are observed at these
523 hydrologically-independent sites, a climate forcing should be considered, with a
524 pervasive shift to a more positive P-E balance after c. 4000 cal yr BP being the most
525 plausible conclusion. However, as discussed above, our approach does not preclude
526 the possibility of long-term peat decay rather than climate determining any millennial
527 scale trends and we point out that an increase in humification with age is what would
528 be expected with progressive anaerobic decay over time. Therefore it is important to
529 evaluate this postulated climate reconstruction against independent climate proxy
530 records from these sites and also from the wider region.

531

532 **6.3. Comparison with other New Zealand Holocene climate records**

533 Holocene pollen records for Kopuatai (Newnham et al., 1995a) and Moanatuatua (Jara
534 et al., 2017) have been interpreted as indicating a mid-Holocene change from
535 comparatively warm, wet climate to drier, possibly frostier climate (Fig. 6). Key
536 indicators for this change are the expansion of pollen of *Agathis australis*, which
537 prefers dry conditions for growth, particularly in spring (Fowler & Boswijk, 2007),
538 and the decline in the frost and drought sensitive *Ascarina lucida*. The *Agathis*
539 *australis* pollen records at Kopuatai (Newnham et al., 1995a) and Moanatuatua (Jara
540 et al., 2017) are insightful. *Agathis* was absent during the early Holocene, but
541 expanded from c. 7000 - 5000 cal yr BP, a pattern evident in other records from the
542 region (e.g. Newnham *et al.*, 1989; 1991; 1995a; 1995b; van den Bos *et al.*, 2018).
543 Dendroclimatological analyses of *Agathis australis* has shown the width of growth
544 rings is strongly linked to ENSO, with wide rings associated with El Niño events
545 (Fowler et al., 2007; 2012) when drier summers typically occur in the Waikato region.

546

547 These assertions are further supported by the pollen-climate reconstructions reported
548 previously from Moanatuatua bog by Jara et al (2017). A pollen-derived moisture
549 index independent of *Agathis* shows a long-term drying trend commencing by ca.
550 7000 cal. yr BP, although persistent below-average values are not observed until c.
551 3500 cal yr BP (Fig. 6). A similar drying trend is reported at Lake Pupuke, Auckland,
552 ~90–130 km to the northwest of the study sites (van den Bos *et al.*, 2018; Fig. 1; Fig.
553 6). At the same site, a Holocene summer temperature reconstruction derived using
554 chironomids also provides informative insight into seasonal climate variability for the
555 region (van den Bos et al., 2018). At Pupuke, reconstructed summer temperatures rise
556 to peak in the mid-late Holocene, despite mean annual temperatures remaining
557 comparatively constant, implying cooler winters (Fig. 6). Similar mean annual
558 temperature patterns are reconstructed for Moanatuatua (Jara et al., 2017; Fig. 6).
559 Taken together, these quantitative climate reconstructions from Auckland and
560 Waikato are consistent with earlier observations for these regions during the late
561 Holocene, and point strongly to comparatively warm, dry summers but cooler winters
562 at that time. Similar conclusions were drawn from a multi-proxy study in southern
563 South Island that incorporated pollen, testate amoebae, and humification analyses
564 (Wilmshurst et al., 2002).

565

566 In contrast to these climate inferences drawn from the Kopuatai and Moanatuatua
567 pollen records and from Pupuke chironomid and pollen records, a climate
568 interpretation of our humification records from these sites would indicate primarily
569 wetter summers during the interval *c.* 5000–2000 cal. yr BP, albeit punctuated at
570 times by phases of dry summers (see below). We conclude therefore that this long-
571 term trend signalling decreasing humification in younger sediments cannot be
572 attributed to regional climate variability and is likely to be more indicative of long-
573 term decay of peat.

574

575 **6.4. Inferred moisture variability at decadal-centennial scales**

576 Turning to the light transmission residuals (Fig. 5), we observe numerous decadal-
577 centennial scale phases in all six records. As these residual values are assumed to be
578 independent of any long-term decay effect, they seem likely to represent shorter-term
579 variability in summer P-E balance along with other, local site factors. A less-than-

580 complete consistency across the records within and between sites suggests that local
581 site factors at times may over-ride a regional climatic signal from an individual
582 humification record. The most likely confounding factor arises from changes in
583 vegetation composition at the core site over time, as has been pointed out for other
584 regions (e.g. Chambers et al., 1997). Marked changes in vegetation composition over
585 time at a particular core site have been reported previously from plant macrofossil
586 analyses at Kopuatai (Newnham et al., 1995a) and Moanatuatua (Haenfling et al.,
587 2015).

588

589 Other complicating factors could arise from specific characteristics of these restiad
590 bog sites. The bog surfaces exhibit patterns of moist swales and intervening drier
591 hummocks (Clarkson et al., 2004; McGlone, 2009) and it has been suggested that
592 these features may migrate across the surface of the bog over time as part of a natural
593 process of growth dynamics and hence independently of climate variability
594 (McGlone, 2009). This process would likely cause variation in the degree of
595 evapotranspiration and hence bog surface wetness experienced between hummocks
596 and swales which would change as these topographic features migrated across the
597 core sites. Also, the extensive Waikato restiad bogs may lack the climate sensitivity
598 of smaller sites, which, together with the significant water holding properties of
599 restionaceae rootlets (Clarkson et al., 2004), may serve to buffer the sites from
600 paleohydrological change.

601

602 Nevertheless, there are some consistent patterns evident between the different
603 humification records which points to broader scale climate processes that at times
604 outweigh these local site factors. All six profiles show pronounced centennial-scale
605 phases of predominantly wetter or drier summers suggesting that strong centennial
606 scale variability in bog surface wetness was a prevalent feature of Holocene climate.
607 Similar conclusions were drawn from the two previous New Zealand studies
608 involving humification analyses, albeit from single peat profiles (McGlone &
609 Wilmshurst, 1999; Wilmshurst et al., 2002). In the next section, we consider the
610 climate forcing implications of these centennial scale shifts in Waikato bog surface
611 wetness.

612

613 **6.5. Climate forcing mechanisms**

614 It is hardly surprising that Holocene climate proxy records from New Zealand display
615 considerable spatio-temporal variability. Strong regional diversity is evident in the
616 modern climate, arising from complex interactions between the main axial mountain
617 ranges and the principal atmospheric circulation systems, played out across a broad
618 latitudinal domain (e.g., Lorrey & Bostock, 2017). These distinctive spatial patterns
619 are often accentuated by short-term climate variability, largely explained by the
620 dynamic interplay between ENSO and SAM and their modulating effect on the
621 Southern Westerly Winds (SWW) (Kidston et al., 2009; Ummenhofer and England,
622 2007). Largely for these reasons, previous explanations of New Zealand Holocene
623 palaeoclimate variation have typically invoked changes in atmospheric circulation
624 patterns operating on a hemispheric scale. Numerous records support the conclusion
625 drawn by the Pole-Equator-Pole II (Asia-Australasian) group that the circum-
626 Antarctic westerlies strengthened and possibly expanded equatorwards during the
627 Late Holocene (Shulmeister *et al.*, 2004; Lamy et al., 2010). Others have suggested
628 intensification of ENSO from the mid-Holocene resulting in highly variable rainfall
629 throughout New Zealand and the occurrence of severe droughts in eastern and
630 southern regions (McGlone et al., 1992, McGlone and Wilmshurst, 1999). Given the
631 interplay between ENSO/SAM and the SWW observed in modern climate today, all
632 of these mechanisms may be relevant to the records presented here but, as
633 precipitation variability today in the Waikato region of northern New Zealand is
634 strongly linked to ENSO cycles (Ummenhofer and England, 2007), this is likely to be
635 a dominant factor.

636

637 In the context of other proxy records from the region, the peat humification records at
638 Moanatuatua and Kopuatai are consistent with the model of ENSO intensification. At
639 these sites today, drier summers and droughts are more likely during El Niño phases,
640 with increased precipitation from strengthened north-easterly rain-bearing winds
641 during La Niña phases. A mid-Holocene transition towards drier summers, but with
642 increasing variability and stronger seasonality including more extreme droughty
643 summers, suggests that a strengthening of both phases of the ENSO cycle occurred. In
644 pollen records, the late Holocene expansion of *Agathis australis* (described earlier)
645 may also be linked to this ENSO strengthening as was first suggested by McGlone et
646 al (1992). More recently, a quantitative precipitation record using carbon isotope

647 ratios from leaves preserved in lake sediments from subtropical eastern Australia
648 (27°S) revealed enhanced centennial-scale ENSO variability with more frequent El
649 Niño event resulting in several dry anomalies after 3200 cal. yr BP (Barr et al., 2019).

650

651 Variation in strength of ENSO is thought to be due to precessional forcing affecting
652 seasonal insolation values at low latitudes (Clement et al., 2001) although some
653 paleoclimate data do not support this contention (Cobb et al., 2013). We suggest a
654 similar driver for the enhanced seasonality evident in these Waikato bog-based
655 records during the late Holocene. The difference between summer (December) and
656 winter (June) insolation values for the approximate latitude of these sites increased
657 progressively through the Holocene to a maximum at *c.* 2000 cal. yr BP. Increasing
658 seasonality of local insolation would have exacerbated the precession-driven inter-
659 annual variations and overall strengthening of ENSO at these sites, promoting
660 frequency of summer drought despite an overall wetter climate over decadal scales. In
661 contrast, during the Early Holocene, reduced seasonality coupled with weaker pole-to-
662 equator temperature gradients are consistent with evidence for weaker ENSO forcing
663 at that time (e.g. Rodbell et al., 1999; Moy et al., 2002).

664

665 At shorter timescales, the strong controls exerted by ENSO cycles on precipitation in
666 the Waikato region today support the contention that they have contributed to the
667 pronounced centennial-scale variability we observe in the humification residuals at
668 both our bog sites. We test this assertion by comparing the Waikato bog humification
669 records with the flagship Holocene record of ENSO events from Laguna Pallcacocha,
670 Ecuador (Moy et al., 2002). For this comparison we have derived a regional
671 humification record by summing the humification residuals for all six records in 100-
672 year bins (Fig. 7). With this approach, we assume the regional climatic signal inherent
673 across the six records is likely to overshadow any individual local site ‘noise’. We test
674 this assumption by comparing the composite regional record with a proxy index for
675 water-table variability derived independently at a different core site at Moanatuatua
676 Bog, using pollen corrosion analysis (Jara et al., 2017). This comparison (Fig. 7)
677 shows a strong match between regional wet (dry) phases inferred from the composite
678 humification record and phases of high (low) water table at Moanatuatua inferred
679 from pollen corrosion.

680

681
682 Turning to the comparison with ENSO, at the centennial scale, the Laguna
683 Pallcacocha record shows four phases of enhanced warm El Niño activity during the
684 timeframe of our humification records (~6200–1700 cal yr BP) when the frequency of
685 these events exceeded ten per century: at 5.7–5.5 cal yr BP, 5.0–4.8 cal yr BP, 3.0–2.8
686 cal yr BP, and 2.6–2.4 cal yr BP. Each of these four phases corresponds with
687 relatively dry phases in northern New Zealand when composite light transmission
688 residuals are approximately at or below average for the interval. Conversely, each of
689 the five wettest Waikato phases inferred from the composite humification record,
690 when summed light transmission residuals are ≥ 2 , correspond to phases of reduced
691 warm El Niño events (≤ 5 per century) when La Niña events can be assumed to be
692 more frequent: at 6.2–6.0 cal yr BP, 4.4–4.2 cal yr BP, 3.5–3.4 cal yr BP, 2.8–2.6 cal
693 yr BP, and 1.9–1.7 cal yr BP. We note that the last interval broadly corresponds with
694 an inferred intense period of La Niña in concert with positive SAM reconstructed
695 from a sedimentological record at Lake Tutira, east-central North Island (Gomez et
696 al., 2012).

697
698 Although the teleconnection between these two records at distant points of the ENSO
699 domain is not perfectly matched, the alignment of the more extreme phases of ENSO
700 activity with Waikato paleohydrology demonstrates the potential of peat humification
701 analyses of Waikato bogs to serve as a proxy for paleo ENSO. Similar assertions
702 have been drawn using peat humification records from northeast Queensland (Turney
703 et al., 2004, Burrows et al., 2014)

704

705 **7.0. Conclusions**

706 There is considerable interest in developing longer-term reconstructions of SWW
707 shifts and associated key modes of climate variability such as SAM and ENSO.
708 However, as recently pointed out by Turney et al. (2017), there is much regional
709 variability in these climate modes whilst the timing of maximum westerly airflow
710 strength and its core latitude may also vary considerably in time and space. Not
711 surprisingly, these complexities raise questions over the value of extending
712 reconstructions from one region to the wider hemisphere (Fletcher and Moreno,
713 2012). On the other hand, if the local climate signatures for the different phases of
714 these climate modes are well understood, and if they can be translated with

715 confidence into local climate proxies that can be shown to vary consistently across
716 multiple well-dated sedimentary records, then regional-hemispheric comparisons are a
717 viable and potentially powerful means of reconstructing these past modes of climate
718 variability.

719

720 The underlying premise to the current study is that a conceptual relationship between
721 peat humification analysis and paleohydrology potentially has an important
722 contribution to this effort. The primary rationale has been to assemble multiple
723 records of peat humification to test their suitability as a proxy for past effective
724 precipitation in northern New Zealand, where precipitation variability is a key
725 manifestation of ENSO cycles. We sought to mitigate some of the confounding
726 factors reported previously for humification analysis by developing robust
727 independent chronologies for each of the six records, based on high resolution, local,
728 ¹⁴C dating, and an independently-derived tephrochronological record, and by targeting
729 two hydrologically separate but ecologically similar raised bogs from the Waikato
730 region. We applied an underpinning rationale that replicability across these records
731 would point strongly to climatic forcing of humification trends over and above other
732 confounding factors.

733

734 Our results suggest that humification records from ombrogenous bogs can provide
735 insight into past climate dynamics but that non-climatic confounding factors must also
736 be critically considered. We argue from comparison with independent climate proxy
737 records that slow anaerobic decomposition of the peat deposits over time rather than
738 climate best explains a long-term trend in humification, despite this trend being
739 observed in all six records. On the other hand, once this decay factor is detrended,
740 replication between records provides a useful approach, both in terms of testing the
741 applicability of the method in a certain region or site, and in developing a level of
742 confidence in any paleoclimate assertions drawn. An important ramification from this
743 study is that a single humification record may not always be reliable for indicating
744 wet-dry shifts at decadal-centennial timescales, as has also been found at other multi-
745 site humification studies (Payne & Blackford, 2008; Amesbury et al., 2012). The most
746 likely confounding local site factors are changing vegetation at the core site over time
747 affecting the composition and decomposition of accumulating peat, which occurred at
748 both sites. Another factor at these sites may be changes in local topography over time.

749

750 Despite these likely local confounding factors, when our six humification records are
751 aggregated at the regional level, they display good correspondence with key phases of
752 the well-documented Holocene ENSO record at Laguna Pallcacocha in the eastern
753 Equatorial Pacific. Within the timeframe common to the two records the most
754 prominent phases of El Niño at Pallcacocha coincide with relatively dry intervals at
755 Waikato, consistent with local signatures of El Niño climate. Conversely, all of the
756 wettest phases in the Waikato record coincide with inferred extensive La Niña phases
757 at Pallcacocha, again consistent with local Waikato signatures of ENSO climate
758 variability. Among the latter, the interval 2.1–1.7 cal ka stands out as a pronounced
759 wet phase in all six humification records, in line with findings from previous work in
760 eastern North Island that invokes sustained La Niña and positive SAM conditions at
761 this time. Other less-pronounced centennial-scale shifts in bog surface wetness are a
762 pervasive feature of all six records with varying degrees of overlap in time, and may
763 arise from other permutations of these predominant climate forcing mechanisms.
764 Future work aimed at showing how these modes of climate variability have operated
765 in the past could be informed by replicated humification records from New Zealand’s
766 raised bogs.

767

768 **Acknowledgements**

769 We thank the Department of Conservation (Hamilton) and Wallace Farm for coring
770 permission and access, and a number of colleagues for valued assistance with field
771 work and laboratory analyses at Plymouth and Waikato universities, in particular Phil
772 Hodges, Annette Rodgers, and other technical staff of the School of Science at
773 University of Waikato. Dr Ganqing Xu (University of Waikato) helped Lowe prepare
774 samples for electron microprobe analyses, which were undertaken by Dr Kathryn
775 Wilson with support from John Patterson (Victoria University of Wellington). Drs
776 Fiona Petchey and Alan Hogg (Waikato Radiocarbon Dating Laboratory) are thanked
777 for assistance with the Waikato dates and Joss Ratcliffe (University of Waikato) for
778 helpful discussion on interpretation of humification records. The AMS radiocarbon
779 dates were funded by the NERC Radiocarbon Facility (Environment) Allocation
780 948.1201. This work was supported by a research grant from the Leverhulme Trust
781 (Grant Ref: RPG-2015-394). The paper is an output also of the EXTRAS project
782 “EXTending TephRAS as a global geoscientific research tool stratigraphically,
783 spatially, analytically, and temporally” led by the International focus group on
784 tephrochronology and volcanism (INTAV) of the Stratigraphy and Chronology
785 Commission (SACCOM) of the International Union for Quaternary Research
786 (INQUA) for 2015-2019. Finally, we are grateful to two referees who provided very
787 useful comments and references that enabled us to improve the paper.

788

789 **References**

790

791 Aaby B, Tauber H. 1975 Rates of peat formation in relation to degree of humification
792 and local environment, as shown by studies of a raised bog in Denmark. *Boreas* **4**: 1-
793 17

794

795 Abram N, Mulvaney R, Vimeux F, Phipps SJ, Turner J, England MH, 2014.
796 Evolution of the Southern Annular Mode during the past millennium. *Nat. Clim.*
797 *Change* **4**: 564–569.

798

799 Alloway BV, Westgate JA, Pillans B, Pearce N, Newnham RM, Byrami M, Aarburg
800 S. 2004. Stratigraphy, age and correlation of middle Pleistocene silicic tephras in the
801 Auckland region, New Zealand: a prolific distal record of TVZ volcanism. *New*
802 *Zealand Journal of Geology & Geophysics* **47**: 447-479

803

804 Amesbury MJ, Barber KE, Hughes PDM. 2012. The relationship of fine-resolution,
805 multi-proxy palaeoclimate records to meteorological data at Fågelmossen, Värmland,
806 Sweden and the implications for the debate on climate drivers of the peat-based
807 record. *Quaternary International* **268**: 77-86

808

809 Amesbury M, Charman DJ, Newnham RM, Loader NJ, Goodrich JP, Royles J,
810 Campbell DI, Keller DE, Baisden T, Roland TP, Gallego-Sala AV, 2015. Can oxygen
811 stable isotopes be used to track precipitation moisture source in vascular plant
812 dominated peatlands? *Earth and Planetary Science Letters* **430**: 149-159.

813

814 Amesbury M, Charman DJ, Newnham RM, Loader NJ, Goodrich JP, Royles J,
815 Campbell DI, Roland TP, Gallego-Sala AV, 2015. Carbon stable isotopes as a
816 palaeoclimate proxy in vascular plant dominated peatlands. *Geochimica et*
817 *Cosmochimica Acta*, 164, 161-174

818

819 Ballinger, M.J. 2003. Developing methods for identifying cryptic tephra in peat cores
820 from the Waikato region, North Island, New Zealand. MRes thesis, University of
821 Plymouth, Plymouth, UK.

822

823 Barber KE. 1981. *Peat stratigraphy and climatic change: a palaeoecological test of*
824 *the theory of cyclic peat bog regeneration*. Balkema, Rotterdam.

825 Barr C, Tibby J, Leng M, Tyler J, Henderson A, Overpeck J, Simpson G, Cole J,
826 Phipps S, Marshall J. 2019. Holocene El Niño–southern Oscillation variability
827 reflected in subtropical Australian precipitation. *Scientific reports* **9**: 1627, 2019.

828 Blackford JJ, Chambers FM. 1993. Determining the degree of peat decomposition for
829 peat-based palaeoclimate studies. *International Peat Journal* **5**: 7-24.

830

831 Borgmark A, Wastegård S. 2008. Regional and local patterns of peat humification in
832 three raised peat bogs in Värmland, south-central Sweden. *GFF* **130**: 161-176.

833

834 Bronk Ramsey C. 2008. Deposition models for chronological records. *Quaternary*
835 *Science Reviews* **27(1-2)**: 42-60.
836
837 Bronk Ramsey C. 2009. Dealing with outliers and offsets in radiocarbon dating.
838 *Radiocarbon* **51(3)**: 1023-1045.
839
840 Campbell DI, Williamson JL. 1997. Evaporation from a raised bog. *Journal of*
841 *Hydrology* **193**: 142-160.
842
843 Campbell DI, Jackson R. 2004. Hydrology of wetlands. In Harding, J.S., Mosley, P.,
844 Pearson, C. and Sorrell, B.K., editors, *Freshwaters of New Zealand, New Zealand*
845 *Hydrological Society and New Zealand Limnological Society, Christchurch*, 20.1-
846 20.14.
847
848 Caseldine C, Baker A, Charman D, Hendon D. 2000. A comparative study of optical
849 properties of NaOH extracts: implications for humification studies. *The Holocene* **10**:
850 649-658.
851
852 Chambers FM, Barber KE, Maddy D, Brew J. 1997. A 5500-year proxy-climate and
853 vegetational record from blanket mire at Talla Moss, Peebleshire, Scotland. *The*
854 *Holocene* **7**: 391-399.
855
856 Chambers FM, Beilman DW, Yu Z. 2011. Methods for determining peat humification
857 and for quantifying peat bulk density, organic matter and carbon content for
858 palaeostudies of climate and peatland carbon dynamics. *Mires and Peat* **7 (7)**: 1-10.
859
860 Chambers FM, Booth RK, De Vleeschouwer F, Lamentowicz M, Le Roux G,
861 Mauquoy D, Nichols JE, van Geel B. 2012. Development and refinement of proxy-
862 climate indicators from peats. *Quaternary International* **268**: 21–33.
863
864 Charman DJ. 2007. Summer water deficit controls on peatland water table changes:
865 implications for Holocene palaeoclimate reconstructions. *The Holocene* **17**: 217-227.
866
867 Clarkson BR. 2002. Swamps, fens and bogs. In Clarkson BD, Merrett M. and Downes
868 T, editors, *Botany of the Waikato*, Waikato Botanical Society, Hamilton, 49-58.
869
870 Clarkson BR, Thompson K, Schipper LA, McLeod M, 1999. Moanatuatua Bog –
871 proposed restoration of a New Zealand restiad peat bog ecosystem. In Streever W,
872 editor, *An international perspective on peatland rehabilitation*, Kluwer, The
873 Netherlands, 127-137.
874
875 Clarkson BR, Schipper LA, Lehmann A. 2004. Vegetation and peat characteristics in
876 the development of lowland and restiad peat bogs, North Island, New Zealand.
877 *Wetlands* **24**: 133-151.
878
879 Clement A, Cane M, Seager R. 2001. An orbitally driven tropical source for abrupt
880 climate change. *Journal of Climatology* **14**: 2369-2375.
881

882 Cobb KM, Westphal N, Sayani HR, Watson JT, Di Lorenzo E, Cheng H, Edwards R.
883 L, Charles CD. 2013. Highly Variable El Niño-Southern Oscillation throughout the
884 Holocene. *Science* **339**: 67–70.
885

886 Cranwell LM. 1939. Native vegetation. Soils and agriculture of part of Waipa County.
887 Dept. of Scientific and Industrial Research, Wellington, pp. 23–29
888 <https://doi.org/10.7931/DL1-SBP-0005>
889

890 Cranwell LM, von Post L. 1936. Post-Pleistocene Pollen Diagrams from the Southern
891 Hemisphere. *Geografiska Annaler* **18**:3-4, 308-347, DOI:
892 10.1080/20014422.1936.11880619
893

894 Clymo RS1984. The limits to peat bog growth. *Philosophical Transactions of the*
895 *Royal Society of London B* **303**, 605-654
896

897 Damaschke, M., Cronin, S.J., Holt, K.A., Bebbington, M.S., Hogg, A.G., 2017. A
898 30,000 yr high-precision eruption history for the andesitic Mt Taranaki, North Island,
899 New Zealand. *Quaternary Research* **87**, 1-23.
900

901 Davoren A. 1978. A survey of New Zealand peat resources. *Water and Soil Technical*
902 *Publication No. 14*, 155 pp.
903

904 de Lange P, Heenan P, Clarkson BD, Clarkson BR. 1999. Taxonomy, ecology, and
905 conservation of *Sporadanthus* (Restionaceae) in New Zealand. *New Zealand Journal*
906 *of Botany* **37**: 413-431.
907

908 de Lange PJ, Lowe DJ, 1990. History of vertical displacement of Kerepehi Fault at
909 Kopuatai bog, Hauraki Lowlands, New Zealand, since c. 10,700 years ago. *New*
910 *Zealand Journal of Geology and Geophysics* **33**: 277-283.
911

912 Edbrooke SW. (compiler) 2001. *Geology of the Auckland area*: Institute of
913 Geological and Nuclear Sciences 1:250,000 Geological Map 3. 1 sheet and 74 pp.
914 IGNS, Lower Hutt.
915

916 Edbrooke SW. (compiler) 2005. *Geology of the Waikato area*. Institute of Geological
917 and Nuclear Sciences 1:250,000 Geological Map 4. 1 sheet and 68 pp. IGNS, Lower
918 Hutt.
919

920 Elliot M, Neall V, Wallace C. 2005. A late Quaternary pollen record from Lake
921 Tangonge, far northern New Zealand. *Reviews of Palaeobotany and Palynology* **136**:
922 143-158.
923

924 Euskirchen ES, Edgar CW, Turetsky MR, Waldrop MP, Harden JW. 2014.
925 Differential response of carbon fluxes to climate in three peatland ecosystems that
926 vary in the presence and stability of permafrost. *J. Geophys. Res. Biogeosciences* **119**:
927 1576–1595. <https://doi.org/10.1002/2014JG002683>
928

929 Fogt RL, Perlwitz J, Monaghan AJ, Bromwich DH, Jones JM, Marshall GJ. 2009.
930 Historical SAM variability. Part II: Twentieth-century variability and trends from
931 reconstructions, observations and the IPCC AR4 models. *J. Clim.* **22**: 5346-5365

932
933 Fowler A, Boswijk G. 2007. Five centuries of ENSO history recorded in Agathis
934 Australis (kauri) tree rings. *PAGES News* **15(2)**: 20-21.
935
936 Fowler A, Boswijk G, Gergis J, Lorrey A. 2007. ENSO history recorded in Agathis
937 australis (kauri) tree rings. Part A: kauri's potential as an ENSO proxy. *International*
938 *Journal of Climatology* **28**: 21 – 35.
939
940 Fowler A, Boswijk G, Lorrey A, Gergis J, Pirie M, McCloskey SPJ, Wunder J, 2012.
941 Multi-centennial tree-ring record of ENSO-related activity in New Zealand. *Nature*
942 *Climate Change* **2**: 172-176.
943
944 Fritz C, Campbell DI, Schipper LA. 2008. Oscillating peat surface levels in a restiad
945 wetland, New Zealand – magnitude and spatiotemporal variability. *Hydrological*
946 *Processes* **22**: 3264-3274.
947
948 Froggatt PC. 1983. Toward a comprehensive Upper Quaternary tephra and ignimbrite
949 stratigraphy in New Zealand using electron microprobe analysis of glass shards. *Quat.*
950 *Res.* **19**: 188-200.
951
952 Garreaud RD, 2007. Precipitation and circulation covariability in the extratropics, *J.*
953 *Clim.* **20(18)**: 4789–4797.
954
955 Gehrels MJ, Lowe DJ, Hazell ZJ, Newnham RM. 2006. A continuous 5300-year
956 Holocene cryptotephrostratigraphic record from northern New Zealand and
957 implications for tephrochronology and volcanic-hazard assessment. *The Holocene* **16**:
958 173-187.
959
960 Gehrels, M.J., Newnham, R.M., Lowe, D.J., Wynne, S., Hazell, Z.J., Caseldine, C.
961 2008. Towards rapid assay of cryptotephra in peat cores: Review and evaluation of
962 selected methods. *Quaternary International* **178**, 68-84.
963
964
965 Gomez B, Carter L, Orpin AR, Cobb K, Page MJ, Trustrum N, Palmer A. 2012.
966 ENSO/SAM interactions during the middle and late Holocene. *The Holocene* **22**: 23–
967 30.
968
969 Goodrich, J. P., Campbell, D. I., Roulet, N. T., Clearwater, M. J., & Schipper, L. A.
970 2015. Overriding control of methane flux temporal variability by water table
971 dynamics in a Southern Hemisphere, raised bog. *Journal of Geophysical Research:*
972 *Biogeosciences* **120(5)**: 819-831. doi:[10.1002/2014JG002844](https://doi.org/10.1002/2014JG002844)
973
974 Goodrich JP, Campbell DI, Schipper LA. 2017. Southern Hemisphere bog persists as
975 a strong carbon sink during droughts. *Biogeosciences* **14**: 4563-4576.
976
977 Haenfling C, Newnham RM, Rees A, Jara I, Homes A, Clarkson B. 2017. Holocene
978 history of a raised bog, northern New Zealand, based on plant cuticles. *The Holocene*
979 **27**: 309-314.
980

- 981 Hartmann, DL, et al. 2013. Observations: Atmosphere and Surface. In Stocker, T. et
982 al. (eds.) *Climate Change 2013: The Physical Science Basis*. Cambridge: CUP, 159-
983 254.
- 984
- 985 Hazell Z, 2004. Holocene palaeoclimate reconstruction from New Zealand peatlands.
986 Unpublished Ph.D. thesis, University of Plymouth, UK.
- 987
- 988 Hodder APW, de Lange PJ, Lowe DJ. 1991. Dissolution and depletion of
989 ferromagnesian minerals from Holocene tephras in an acid bog, New Zealand, and
990 implications for tephra correlation. *Journal of Quaternary Science* **6**: 195-208.
- 991
- 992 Hogg AG, Higham TFG, Lowe DJ, Palmer J, Reimer P, Newnham RM. 2003. A
993 wiggle-match date for Polynesian settlement of New Zealand. *Antiquity* **77**: 116-125.
- 994
- 995 Hogg AG, Lowe DJ, Palmer JG, Boswijk G, Bronk Ramsey C, 2012. Revised
996 calendar date for the Taupo eruption derived by 14C wiggle-matching using a New
997 Zealand kauri 14C calibration data set. *The Holocene* **22**: 439-449.
998 10.1177/0959683611425551.
- 999
- 1000 Hogg, A.G., Hua, Q., Blackwell, P.G., Niu, M., Buck, C.E., Guilderson, T.P., Heaton,
1001 T.J., Palmer, J.G., Reimer, P.J., Reimer, R.W., Turney, C.S.M., & Zimmerman, S.
1002 R.H. 2013. SHCal13 Southern Hemisphere Calibration, 0-50,000 Years cal BP.
1003 *Radiocarbon* **55(4)**: 1889–1903.
- 1004
- 1005 Hughes PDM, Mallon G, Essex HJ, Amesbury MJ, Charman DJ, Blundell A,
1006 Chambers FM, Daley TJ, Mauquoy D. 2012. The use of k-values to examine plant
1007 ‘species signals’ in a peat humification record from Newfoundland. *Quaternary*
1008 *International* **268**:156-165
- 1009
- 1010 Jara, I.A., Newnham, R.M., Alloway, B.V., Wilmshurst, J.M., Rees, A.B.H., 2017.
1011 Pollen-based temperature and precipitation records of the past 14,600 years in
1012 northern New Zealand (37°S) and their linkages with the Southern Hemisphere
1013 atmospheric circulation. *The Holocene* **27(1)**: 1756-1768. DOI:
1014 10.1177/0959683617708444
- 1015
- 1016 Jarosewich, E., 2002. Smithsonian microbeam standards. *Journal of Research of the*
1017 *National Institute of Standards and Technology* **107**: 681-685.
- 1018
- 1019 Jarosewich, E., Nelen, J.A., Norberg, J.A., 1980. Reference samples for electron
1020 microprobe analysis. *Geostandards Newsletter* **4**: 43-47.
- 1021
- 1022 Jones JM, Gille ST, Goosse H, et al., 2016. Assessing recent trends in high-latitude
1023 Southern Hemisphere surface climate. *Nature Climate Change* **6**: 917-926. doi:
1024 10.1038/nclimate3103
- 1025
- 1026 Kidston, J., Renwick, J. A., McGregor, J., 2009. Hemispheric-scale seasonality of the
1027 Southern Annular Mode and impacts on the climate of New Zealand. *J. Climate*, **22**,
1028 4759–4770.
- 1029

1030 Kottek M, Grieser J, Beck C, Rudolf B, Rubel F. 2006. World map of the Köppen-
1031 Geiger climate classification updated. *Meteorologische Zeitschrift* 15, 259-263.
1032
1033 Kuder, T., Krüge, M., Shearer, J., Miller, S. 1998. Environmental and botanical
1034 controls on peatification – a comparative study of two New Zealand restiad bogs
1035 using Py-Gc/Ms, petrography and fungal analysis. *International Journal of Coal*
1036 *Geology* 37, 3-27.
1037
1038 Lafleur PM, Moore TR, Roulet NT, Froelking S. 2005. Ecosystem respiration in a cool
1039 temperate bog depends on peat temperature but not water table. *Ecosystems*: 8, 619–
1040 629. <https://doi.org/10.1007/s10021-003-0131-2>
1041
1042 Lamy F, Kilian R, Arz HW, Francois JP, Kaiser J, Prange M, Steinke T. 2010.
1043 Holocene changes in the position and intensity of the southern westerly wind belt.
1044 *Nature Geoscience* 3(10), 695-699.
1045
1046 Langdon, PG, Hughes, PDM, Brown AG. 2012 Peat stratigraphy and climate change.
1047 *Quaternary International* 268:1-8.
1048
1049 Lorrey AM, Vandergoes MJ, Almond PC, Renwick JR, Stephens T, Bostock H,
1050 Mackintosh A, Newnham RM, Williams PW, Ackerley D, Neil H, Fowler AM. 2012.
1051 Palaeocirculation across New Zealand during the last glacial maximum at ~21 ka.
1052 *Quat Sci Rev* 36:189-213.
1053
1054 Lorrey, A.M., Bostock, H. 2017. The climate of New Zealand through
1055 the Quaternary. In: Shulmeister, J. (ed.), *Landscape and Quaternary Environmental*
1056 *Change in New Zealand*, Atlantis Advances in Quaternary Science 3, 67-139.
1057 DOI 10.2991/978-94-6239-237-3_367
1058
1059 Lowe DJ, 1988. Stratigraphy, age, composition, and correlation of late Quaternary
1060 tephra interbedded with organic sediments in Waikato lakes, North Island, New
1061 Zealand. *NZ. J. Geol. Geophys.* 31: 125-165.
1062
1063 Lowe DJ. 2011. Tephrochronology and its application: a review. *Quaternary*
1064 *Geochronology* 6: 107-153.
1065
1066 Lowe DJ, Newnham RM, Ward CM. 1999: Stratigraphy and chronology of a 15 ka
1067 sequence of multi-sourced silicic tephra in a montane peat bog, eastern North Island,
1068 New Zealand. *New Zealand Journal of Geology and Geophysics* 42: 565-579.
1069
1070 Lowe DJ, Shane PAR, Alloway BV, Newnham RM. 2008: Fingerprints and age
1071 models for widespread New Zealand tephra marker beds erupted since 30,000 years
1072 ago: a framework for NZ-INTIMATE. *Quaternary Science Reviews* 27: 95-126.
1073
1074 Lowe, D.J., Blaauw, M., Hogg, A.G., Newnham, R.M. 2013. Ages of 24 widespread
1075 tephra erupted since 30,000 years ago in New Zealand, with re-evaluation of the
1076 timing and palaeoclimatic implications of the late-glacial cool episode recorded at
1077 Kaipo bog. *Quaternary Science Reviews* 74: 170-194.
1078

1079 Lowe, D.J., Pearce, N.J.G., Jorgensen, M.A., Kuehn, S.C., Tryon, C.A., Hayward,
1080 C.L. 2017. Correlating tephras and cryptotephras using glass compositional analyses
1081 and numerical and statistical methods: review and evaluation. *Quaternary Science*
1082 *Reviews* **175**: 1-44.

1083
1084 Maggs G. 1997. Hydrology of the Kopuatai peat dome. *New Zealand Journal of*
1085 *Hydrology* **36**: 147-172.

1086
1087 Manville, V., Wilson, C.J.N. 2004. The 26.5 ka Oruanui eruption, New Zealand: a
1088 review of the roles of volcanism and climate in the post-eruptive sedimentary
1089 response. *N.Z. Journal of Geology and Geophysics* **47**: 525-547

1090
1091 Marshall GJ. 2003. Trends in the southern annular mode from observations and
1092 reanalyses. *J. Climate* **16**, 4134-4143.

1093
1094 McCormac F, Hogg A, Blackwell P, Buck C, Higham T, Reimer P. 2004. SHCal04
1095 Southern Hemisphere calibration, 0-11.0 cal. kyr BP. *Radiocarbon* **46**: 1087-1092.

1096
1097 McGlone MS. 1988: New Zealand. In Huntley B, Webb T, editors, *Vegetation*
1098 *history: handbook of vegetation science Volume 7*. Kluwer Academic Publishers, 557-
1099 599.

1100
1101 McGlone MS. 2009. Postglacial history of New Zealand wetlands and implications
1102 for their conservation. *New Zealand Journal of Ecology* **33**: 1-23.

1103
1104 McGlone MS, Kershaw AP, Markgraf, V. 1992. El Niño/Southern Oscillation
1105 climatic variability in Australasian and South American paleoenvironmental records.
1106 In Diaz H, Markgraf V, editors, *El Niño: historical and paleoclimatic aspects of the*
1107 *Southern Oscillation*. University of Arizona Press, 435-462.

1108
1109 McGlone MS, Moar NT, 1977. The Ascarina decline and post-glacial climatic change
1110 in New Zealand. *New Zealand Journal of Botany* **15**, 485-489.

1111
1112 McGlone MS, Turney CSM, Wilmshurst JM. 2004. Late-glacial and Holocene
1113 vegetation and climatic history of the Cass basin, central south island, New Zealand.
1114 *Quaternary Res.* **62**: 267–279. doi: 10.1016/j.yqres.2004. 09.003

1115
1116 McGlone MS, Wilmshurst JM. 1999. A Holocene record of climate, vegetation
1117 change and peat bog development, east Otago, South Island, New Zealand. *Journal of*
1118 *Quaternary Science* **14**(3): 239-254.

1119
1120 McGlone MS, Richardson SJ, Burge OR, Perry GLW, Wilmshurst JM. 2017.
1121 Palynology and the Ecology of the New Zealand Conifers. *Front. Earth Sci.* **5**:94. doi:
1122 10.3389/feart.2017.00094

1123
1124 Morgan TJ, Herod AA, Brain SA, Chambers FM, Kandiyoti R. 2005. Examination of
1125 soil contaminated by coal-liquids by size-exclusion chromatography in 1-methyl-2-
1126 pyrrolidinone solution to evaluate interference from humic and fulvic acids and
1127 extracta from peat *Journal of Chromatography* **1095**: 81-88.

1128

- 1129 Moy CM, Seltzer GO, Rodbell DT, Anderson DM. 2002. Variability of El
 1130 Niño/Southern Oscillation activity at millennial timescales during the Holocene
 1131 epoch. *Nature* **420(6912)**: 162–165
 1132
- 1133 Newnham RM, Lowe DJ, Green JD. 1989. Palynology, vegetation and climate of the
 1134 Waikato lowlands, North Island, since c. 18,000 years ago. *Journal of the Royal
 1135 Society of New Zealand* **19**: 127-150.
 1136
- 1137 Newnham RM, Lowe DJ. 1991. Holocene vegetation and volcanic activity, Auckland
 1138 Isthmus, New Zealand. *Journal of Quaternary Science* **6**: 177-193.
 1139
- 1140 Newnham RM, Ogden J, Mildenhall DC, 1993. Late Pleistocene vegetation history of
 1141 the Far North of New Zealand. *Quaternary Research* **39**: 361-372.
 1142
- 1143 Newnham RM, de Lange P, Lowe DJ. 1995a. Holocene vegetation, climate and
 1144 history of a raised bog complex, northern New Zealand based on palynology, plant
 1145 macrofossils and tephrochronology. *The Holocene* **5(3)**: 267-282.
 1146
- 1147 Newnham RM, Lowe DJ, Wigley GNA. 1995b. Late Holocene palynology and
 1148 palaeovegetation of tephra-bearing mires at Papamoa and Waihi Beach, western Bay
 1149 of Plenty, North Island, New Zealand. *Journal of Royal Society of New Zealand* **25**:
 1150 283-300
 1151
- 1152 Newnham RM, Lowe DJ, McGlone MS, Wilmshurst JM, Higham T. 1998: The
 1153 Kaharoa Tephra as a critical datum for earliest human impact in northern New
 1154 Zealand. *Journal of Archaeological Science* **25**: 533-544.
 1155
- 1156 Newnham RM, Lowe DJ, Alloway BV. 1999. Volcanic hazards in Auckland New
 1157 Zealand: a preliminary assessment of the threat posed by central North Island silicic
 1158 volcanism based on the Quaternary tephrostratigraphical record. In Firth C, McGuire
 1159 WJ (eds) *Volcanoes in the Quaternary*, Geological Society, London, Special
 1160 Publications **161**: 27-45.
 1161
- 1162 Newnham RM, Vandergoes MJ, Sykes E, Carter L, Wilmshurst JM, Lowe, D.J.,
 1163 McGlone MS, Sandiford A. 2012. Does the bipolar seesaw extend to the southern
 1164 mid-latitudes? *Quaternary Science Reviews* **36**: 214-222
 1165
- 1166 NIWA 2009. Climate summaries for 1971-2000 period (Hamilton). CliFlo National
 1167 Institute of Water and Atmospheric Research National Climate Database on the Web.
 1168 <http://CliFlo.niwa.co.nz/>. Retrieved 19 Feb, 2009.
 1169
- 1170 Ogden J, Newnham RM, Palmer JG, Serra R, Mitchell ND, 1993. Climatic
 1171 implications of macro-and micro-fossil assemblages from late Pleistocene deposits in
 1172 northern New Zealand. *Quaternary Research* **39**: 107-119
- 1173 Payne RJ, Blackford JJ. 2009. Peat humification and climate change: a multi-site
 1174 comparison from mires in south-east Alaska. *Mires and Peat* **3**: Art. 9. (Online:
 1175 <http://www.mires-and-peat.net/pages/volumes/map03/map0309.php>)
- 1176

1177 Persaud M, Villamor P, Berryman KR, Ries W, Cousins WJ, Litchfield N, Alloway
1178 BV. 2016. The Kerepehi Fault, Hauraki Rift, North Island, New Zealand: active fault
1179 characterisation and hazard. *New Zealand Journal of Geology and Geophysics* **59**:
1180 117-135.

1181
1182 Pronger, J., Schipper, L.A., Hill, R.B., Campbell, D.I., McLeod, M. 2014. Subsidence
1183 rates of drained agricultural peatlands in New Zealand and the relationship with time
1184 since drainage. *Journal of Environmental Quality* **43**: 1442-1449.

1185
1186 Ratcliffe JL, Campbell DI, Clarkson BR, Wall AM, Schipper LA. 2019. Water table
1187 fluctuations control CO₂ exchange in wet and dry bogs through different mechanisms.
1188 *Science of the Total Environment* **655**: 1037-1046.
1189 <https://doi.org/10.1016/j.scitotenv.2018.11.151>

1190
1191 R Core Team, 2016. R: A language and environment for statistical computing. R
1192 Foundation for Statistical Computing, Vienna, Austria. URL [https://www.R-](https://www.R-project.org/)
1193 [project.org/](https://www.R-project.org/).

1194
1195 Renwick JA. 2005. Persistent positive anomalies in the Southern Hemisphere
1196 circulation. *Monthly Weather Review* **133(4)**: 977–988.

1197
1198 Rodbell DT, Seltzer G.O., Anderson DM, Abbott MB, Enfield DB, Newman JH.
1199 1999. An 15,000-year record of El Niño-driven alluviation in southwestern Ecuador.
1200 *Science* **283**: 516– 520.

1201
1202 Roos-Barraclough F, van der Knaap W, van Leeuwen J, Shotyk W. 2004. A late-
1203 glacial and Holocene record of climatic change from a Swiss peat humification
1204 profile. *The Holocene* **14**: 7–19.

1205
1206 Salinger MJ; Mullan AB. 1999. New Zealand climate: Temperature and precipitation
1207 variations and their links with atmospheric circulation 1930-1994. *International*
1208 *Journal of Climatology* **19**:1049-1071.

1209
1210 Schipper LA, McLeod M. 2002. Subsidence rates and carbon losses in peat soils
1211 following conversion to pasture in the Waikato region, New Zealand. *Soil Use and*
1212 *Management* **18**: 91-93.

1213
1214 Selby MJ, Lowe DJ. 1992. The middle Waikato Basin and hills. In Soons JM, Selby
1215 MJ, editors, *Landforms of New Zealand*. Second Edition. Auckland, Longman Paul,
1216 233-255.

1217
1218 Shearer J. 1997. Natural and anthropogenic influences on peat development in
1219 Waikato/Hauraki Plains restiad bogs. *Journal of the Royal Society of New Zealand* **27**:
1220 295-313.

1221
1222 Shulmeister J, Goodwin I, Renwick J, Harle K, Armand L, McGlone MS, Cook E,
1223 Dodson J, Hesse PP, Mayewski P, Curran M. 2004. The Southern Hemisphere
1224 westerlies in the Australasian sector over the last glacial cycle: a synthesis.
1225 *Quaternary International* **118-119**: 23-53.

1226

- 1227 Sparks RJ, Melhuish WH, McKee JWA, Ogden J, Palmer JG. 1995. ^{14}C calibration in
 1228 the Southern Hemisphere and the date of the last Taupo eruption: evidence from tree-
 1229 ring sequences. *Radiocarbon* **37**: 155-163.
 1230
- 1231 Sparks RJ, Graham IJ, Morgenstern U. 2008. Cosmic chronometers. In Graham, I.J.,
 1232 chief editor, A continent on the move: New Zealand geoscience into the 21st century,
 1233 *Geological Society of New Zealand, Miscellaneous Publication* **124**: 64-67. Lower
 1234 Hutt.
 1235
- 1236 Telford R, Heegaard E, Birks H. 2004a. All age-depth models are wrong: but how
 1237 badly? *Quaternary Science Reviews* **23**: 1-5.
 1238
- 1239 Telford R, Heegaard E, Birks H. 2004b. The intercept is a poor estimate of a
 1240 calibrated radiocarbon age. *The Holocene* **14**: 296-298.
 1241
- 1242 Thompson M, Campbell D, Spronken-Smith R. 1999. Evaporation from natural and
 1243 modified raised peat bogs in New Zealand. *Agricultural and Forest Meteorology* **95**:
 1244 85-98.
 1245
- 1246 Thompson DW, Solomon JS, Kushner PJ, England MH, Grise KM, Karoly DJ. 2011.
 1247 Signatures of the Antarctic ozone hole in Southern Hemisphere surface climate
 1248 change. *Nature Geoscience* **4**: 741-749.
 1249
- 1250 Turney CSM, Wilmshurst JM, Jones RT, Wood JR, Palmer JG, Hogg AG, Thomas Z.
 1251 2017. Reconstructing atmospheric circulation over southern New Zealand:
 1252 Establishment of modern westerly airflow 5500 years ago and implications for
 1253 Southern Hemisphere Holocene climate change. *Quaternary Science Reviews* **159**:
 1254 77-87.
 1255
- 1256 Ummenhofer CC, England MH. 2007. Interannual extremes in New Zealand
 1257 precipitation linked to modes of Southern Hemisphere climate variability. *Journal of*
 1258 *Climate* **20**: 5418-5440
 1259
- 1260 van den Bos V, Rees ABH, Newnham RM, Vandergoes MJ, Wilmshurst JM,
 1261 Augustinus PC. 2018. Holocene temperature, humidity and seasonality in northern
 1262 New Zealand linked to Southern Hemisphere summer insolation. *Quaternary Science*
 1263 *Reviews* **201**: 77-88
 1264
- 1265 Wagstaff SJ, Clarkson BR. 2012. Systematics and ecology of the Australasian genus
 1266 *Empodisma* (Restionaceae) and description of a new species from peatlands in
 1267 northern New Zealand. *PhytoKeys* **13**: 39-79.
 1268
- 1269 Wang C, Cai W. 2013. Climate-change impact on the 20th-century relationship
 1270 between the Southern Annular Mode and global mean temperature. *Nat. Sci. Rep.* **3**:
 1271 DOI:10.1038/srep02039.
 1272
- 1273 Williams PW, King DNT, Zhao J-X, Collerson KD. 2004. Speleothem master
 1274 chronologies: combined Holocene ^{18}O and ^{13}C records from the North Island of New
 1275 Zealand and their palaeoenvironmental interpretation. *The Holocene* **14**: 194-208.
 1276

- 1277 Wilmshurst, J.M., McGlone, M.S. 1996. Forest disturbance in the central North
1278 Island, New Zealand, following the 1850 BP Taupo eruption. *The Holocene* 6, 399-
1279 411.
- 1280
- 1281 Wilmshurst JM, McGlone MS, Charman DJ. 2002. Holocene vegetation and climate
1282 change in southern New Zealand: linkages between forest composition and
1283 quantitative surface moisture reconstructions from an ombrogenous bog. *Journal of*
1284 *Quaternary Science* **17**: 653-666.
- 1285
- 1286 Yeloff D, Mauquoy D. 2006. The influence of vegetation composition on peat
1287 humification: implications for palaeoclimatic studies. *Boreas* **35**: 662-673.
- 1288

1289 **Figure Captions**

1290

1291 **Figure 1.** *a)* Regional setting of New Zealand in southwest Pacific Ocean, showing
1292 principle atmospheric circulation systems and ocean currents; *b)* part of North Island
1293 with site locations; *c)* and *d)* locations of coring sites at Kopuatai bog and
1294 Moanatuatua bog, respectively. Elevations (triangles) are in metres above sea level.

1295

1296 **Figure 2.** Stratigraphy of peat cores at Kopuatai and Moanatuatua showing positions
1297 of tephra and cryptotephra in them (ages are given in Table 1) along with ¹⁴C
1298 sampling positions (laboratory codes and other details are given in Table 4).

1299 ^aStratigraphy after Gehrels et al. (2006)

1300 ^bGrid reference of the New Zealand Topo50 series (1: 50,000)

1301 ^cIdentification after Ballinger (2003)

1302 ^dIdentification after Gehrels et al. (2008); other identifications after Hazell (2004)

1303 ^eThese two ¹⁴C samples were taken from an immediately adjacent core (at BE34
1304 090001) (Hazell, 2004)

1305

1306 **Figure 3.** Linearly-interpolated age-depth models for Kopuatai (*a*) and Moanatuatua
1307 (*b*). Tephra ages are indicated by tephra names, and AMS radiocarbon ages by lab
1308 code. Error bars indicate radiocarbon calibration errors (2-sigma ranges).

1309

1310 **Figure 4.** Corrected light transmission plotted against age for (*a*) the three Kopuatai
1311 cores and (*b*) the three Moanatuatua cores. Bolder curves indicate three-point running
1312 mean.

1313

1314 **Figure 5.** Light transmission residuals averaged in 100-year bins for *a)* three Kopuatai
1315 cores, 6200–1700 cal yr BP and *b)* three Moanatuatua cores, 7000–1700 cal yr BP.
1316 Each bar consists of 3 segments, each representing the average light transmission
1317 value for that period at one core site.

1318

1319 **Figure 6.** Comparison of Holocene climate proxy records from Waikato and
1320 Auckland for the interval 16,000 yr BP to present. From top to bottom, period of
1321 *Agathis australis* expansion at Kopuatai Bog (Newnham et al., 1995a); composite
1322 light transmission records for Kopuatai and Moanatuatua bogs (data, this study, Fig 4)

1323 with red curves indicating LOWESS smoother with span = 0.25; Pollen Moisture
1324 Index (PMI) derived at Moanatuatua Bog (Jara et al., 2017); PMI derived at Lake
1325 Pupuke, Auckland (van den Bos et al., 2018); period of *Agathis australis* expansion at
1326 Lake Pupuke (van den Bos et al., 2018); Mean annual Temperature (MAT) derived at
1327 Moanatuatua Bog (Jara et al., 2017); MAT derived at Lake Pupuke (van den Bos et
1328 al., 2018); Mean Summer Temperature derived at Lake Pupuke (van den Bos et al.,
1329 2018); summer insolation at 37 °C (van den Bos et al., 2018).

1330

1331 Figure 7. Comparison of warm ENSO (El Niño) events record from Lake Pallcacocha,
1332 Ecuador (Moy et al., 2002) with a composite Waikato bog humification record
1333 derived as the sum of six individual light transmission residuals records from
1334 Kopuatai and Moanatuatia bogs (this study), and water table extremes derived from
1335 pollen corrosion analysis at Moanatauatua bog (Jara et al., 2017). Vertical green bands
1336 indicate extended wet phases in Waikato bogs when summed light transmission
1337 residuals are ≥ 2 . Vertical yellow bands indicate extended El Niño phases (manifest in
1338 Waikato as dry phases) when warm ENSO events at Lake Palcacocha ≥ 10 per 100
1339 yrs.

1340

1341

1342

1343 *For Table Captions - please see file with tables*

1344

1345 **Supporting Information**

1346

1347 **Humification correction for mineral content**

1348

1349 Peat samples containing mineral (inorganic) matter ('contamination') are likely to
1350 affect light transmission readings. The presence of mineral matter lowers the organic
1351 proportion of the peat sample resulting in a reduction in the amount of extracted
1352 humic acid and hence higher light transmission values. When the environmental
1353 factors relating to the peat forming process are the primary consideration, as is the
1354 case here, the higher light transmission values for such samples may be misleading.
1355 To overcome this problem, Blackford and Chambers (1993) suggested a linear
1356 correction for light transmission values on peat samples containing mineral matter,
1357 which was subsequently revised by Chambers et al. (2011).

1358

1359 Whilst processing the peat samples in this study, it became evident that enhanced light
1360 transmission was occurring as a result of abundant glass shards representing
1361 cryptotephra deposits in the stratigraphy and that the effect was non-linear. An
1362 experiment was devised to test the relationship between mineral content and light
1363 transmission, and to quantify more accurately the effect of highly minerogenic peats
1364 on light transmission readings. As a result, we have developed a revised correction
1365 procedure based on an exponential relationship between light transmission and
1366 mineral 'contamination', to enable the calculation of light transmission values that
1367 reflect the peat forming process, independently of mineral matter. We applied this
1368 correction in the humification analyses in this study.

1369

1370 Method

1371 Test samples were made using typical *Empodisma*-dominated peat from Kopuatai
1372 Bog with a small amount of background mineral content (2.24% from the loss-on-
1373 ignition [LOI] measurement). Samples were mixed with fine, dried silica sand (Grade
1374 HH) then dried, ground to powder in a Specamill, and thoroughly mixed until
1375 homogeneous. Samples of varying proportions of peat and sand were then made and
1376 weighed. For each of these samples, three replicates were measured for light
1377 transmission, LOI and total organic carbon (TOC). LOI was measured, along with
1378 TOC, as this is the standard technique regularly used for determining the organic

1379 content of samples in determining their correction equation. Thus, the correction can
1380 therefore be applied to either of these indices of organic content.

1381

1382 Results

1383 We found a non-linear relationship between mineral content and light transmission (SI
1384 Fig 1).

1385

1386 **SI Fig 1 here*

1387

1388 The results of the experimental data described the exponential curve:

1389

1390 (1) light transmission = $17.855e^{(0.0171 * \text{mineral content})}$ (SI Fig 1)

1391

1392 From the exponential relationship ($y = ae^{bx}$) it was then possible to calculate a and b
1393 for any given peat sample by solving equations:

1394

1395 (2)
$$b = \frac{\ln y_0 - \ln y_e}{x_0 - x_e}$$

1396

1397 (3)
$$a = \frac{y_0}{\exp(bx_0)}$$

1398

1399 where: x_0 = the mineral content of the sample,

1400 x_e = 100,

1401 y_0 = the light transmission value of the sample,

1402 and y_e = 100.

1403

1404 Correcting for mineral content could then be done on *any* data point – where a is the
1405 corrected light transmission for the sample if it contained no mineral matter.

1406

1407 Results for TOC also showed an exponential relationship with light transmission (SI
1408 Fig 2)

1409 **SI Fig 2 here*

1410

1411 To calculate the corrected light transmission for samples on which TOC, not LOI, had
1412 been measured, the LOI values would have to be replaced using the relationship
1413 between TOC and LOI (SI Fig 3).

1414

1415 **SI Fig 3 here*

1416

1417 These two variables, LOI and TOC, were related linearly ($r^2 = 0.9983$) :

1418

1419 (4)
$$\text{mineral content} = 100.47 - 1.7971 \times \text{TOC}$$

1420

1421 Hence, for a TOC measured sample, x_0 in equations (2) and (3) can be replaced such
1422 that:

1423

1424 (5)
$$b = \frac{\ln y_0 - \ln y_e}{(100.47 - 1.7971x) - x_e}$$

1425

1426 (6)
$$a = \frac{y_0}{\exp(b(100.47 - 1.7971x))}$$

1427

1428 These formulae could then be applied to any peat humification light transmission
1429 result of known LOI or TOC.

1430

1431 **Supporting Information figure captions**

1432

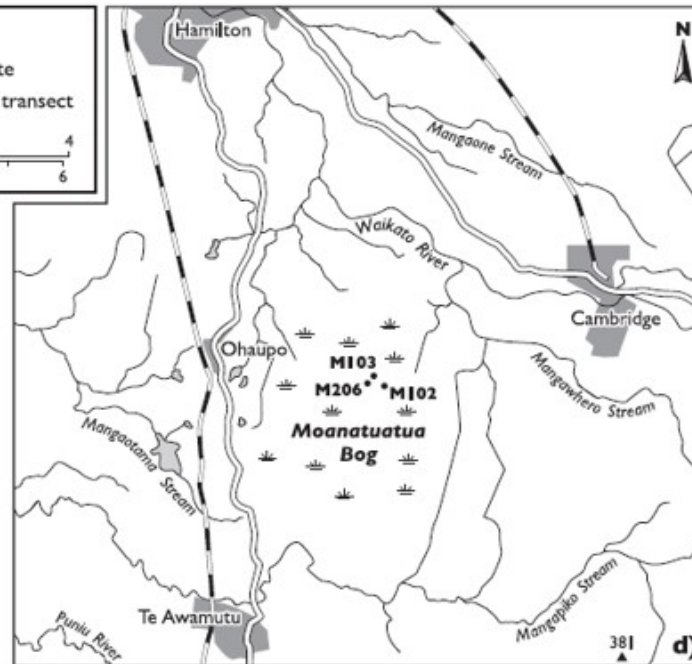
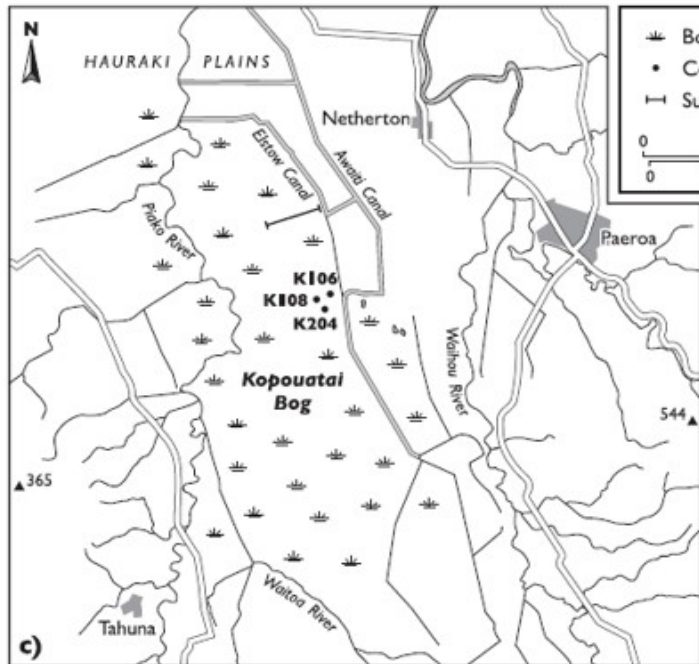
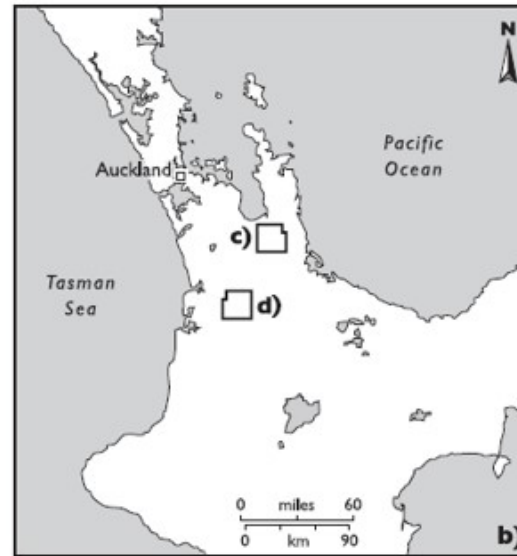
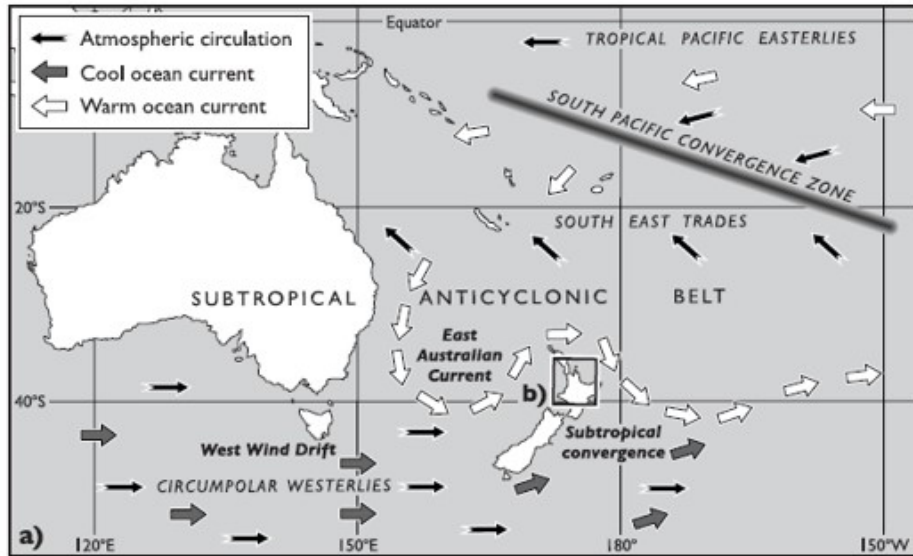
1433 **Figure SI1.** Light transmission plotted against mineral content (calculated from LOI)
1434 for experimental samples.

1435

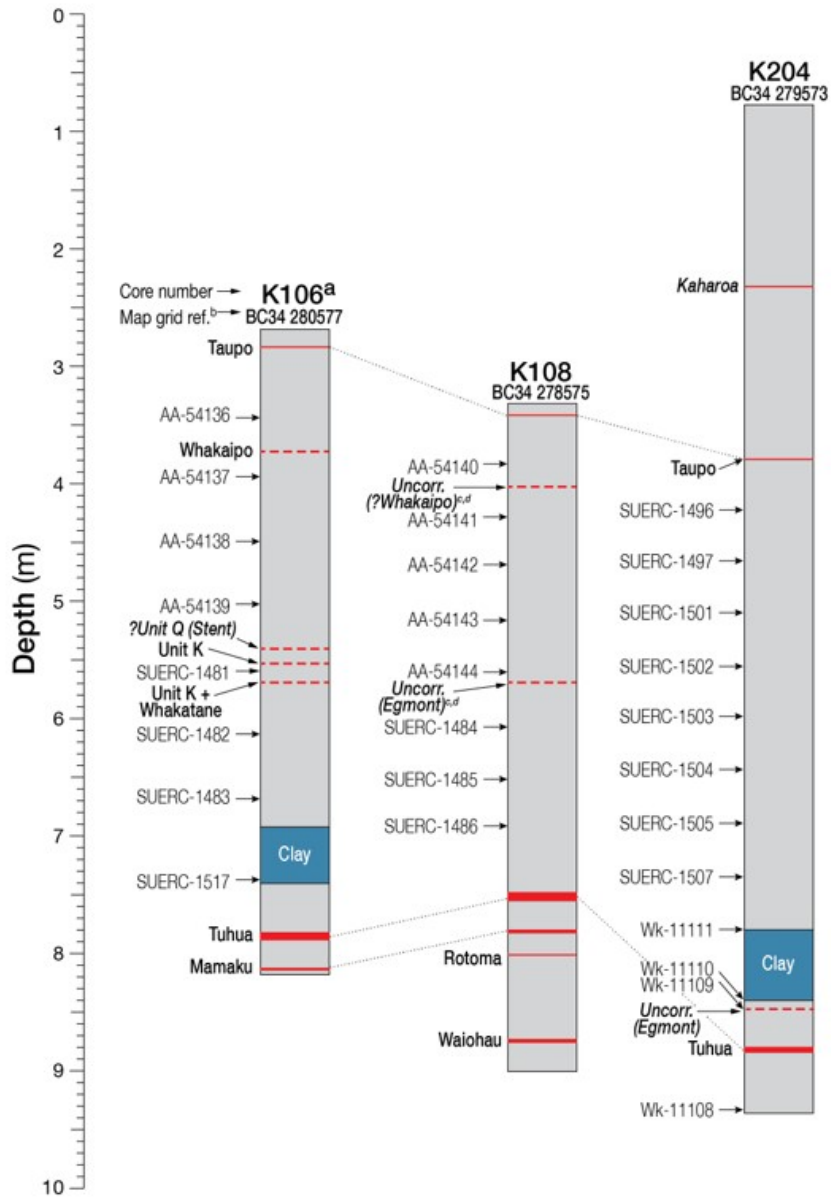
1436 **Figure SI2.** Light transmission plotted against TOC for experimental samples (note
1437 reversal of x axis).

1438

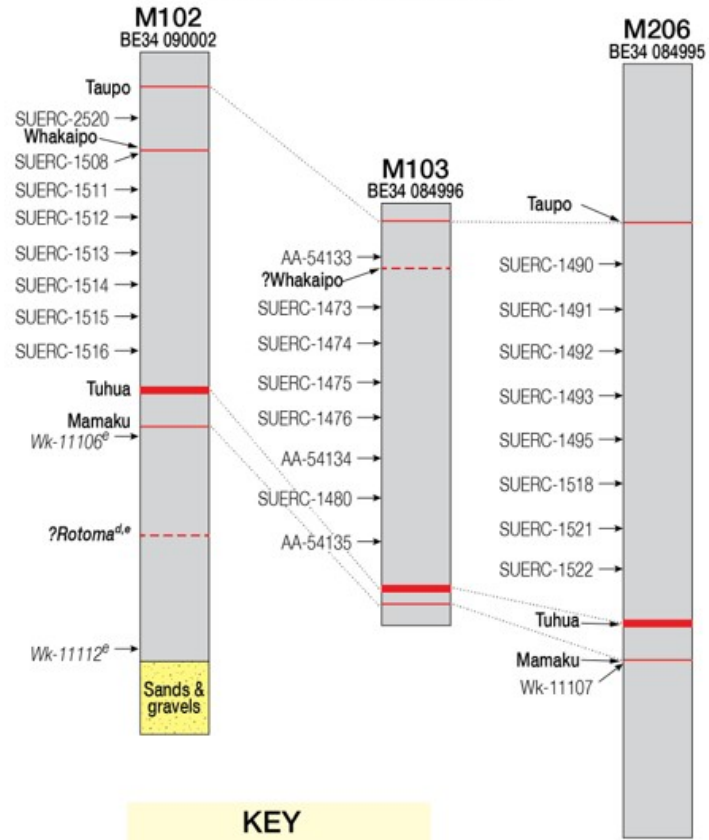
1439 **Figure SI3.** The relationship between TOC and mineral content (expressed as 100-
1440 LOI) for experimental samples.



Kopouatai Bog

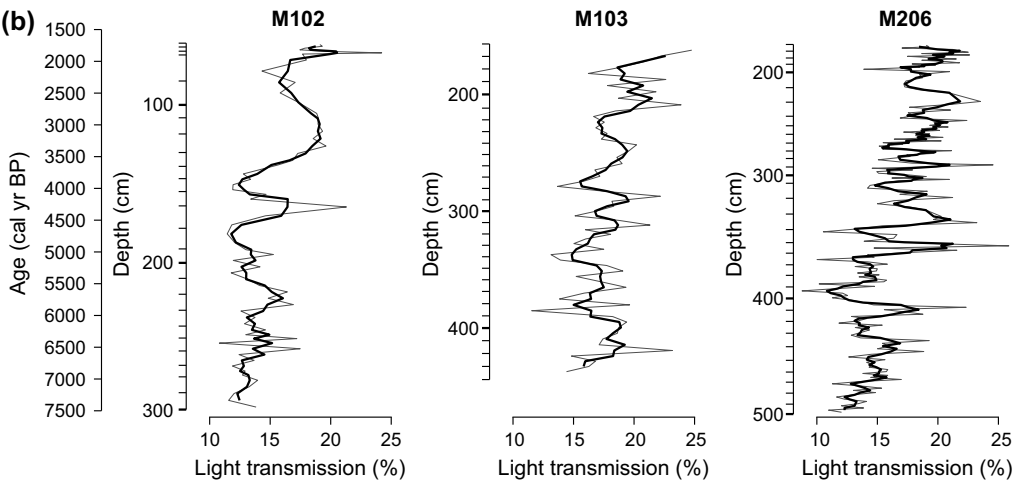
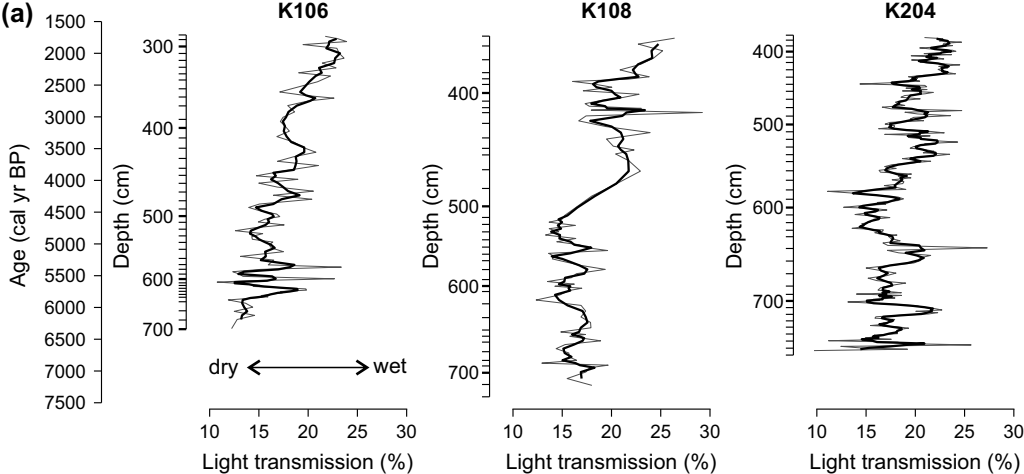


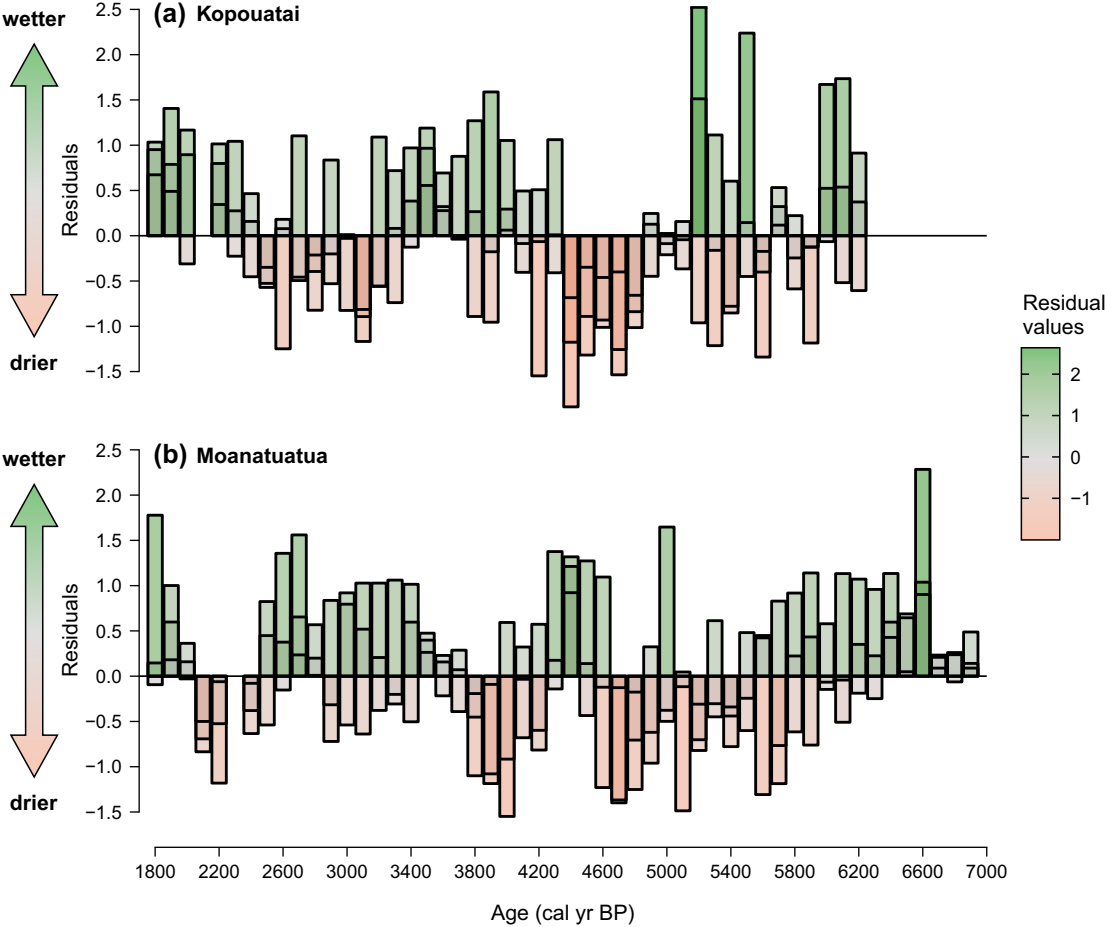
Moanatuatua Bog

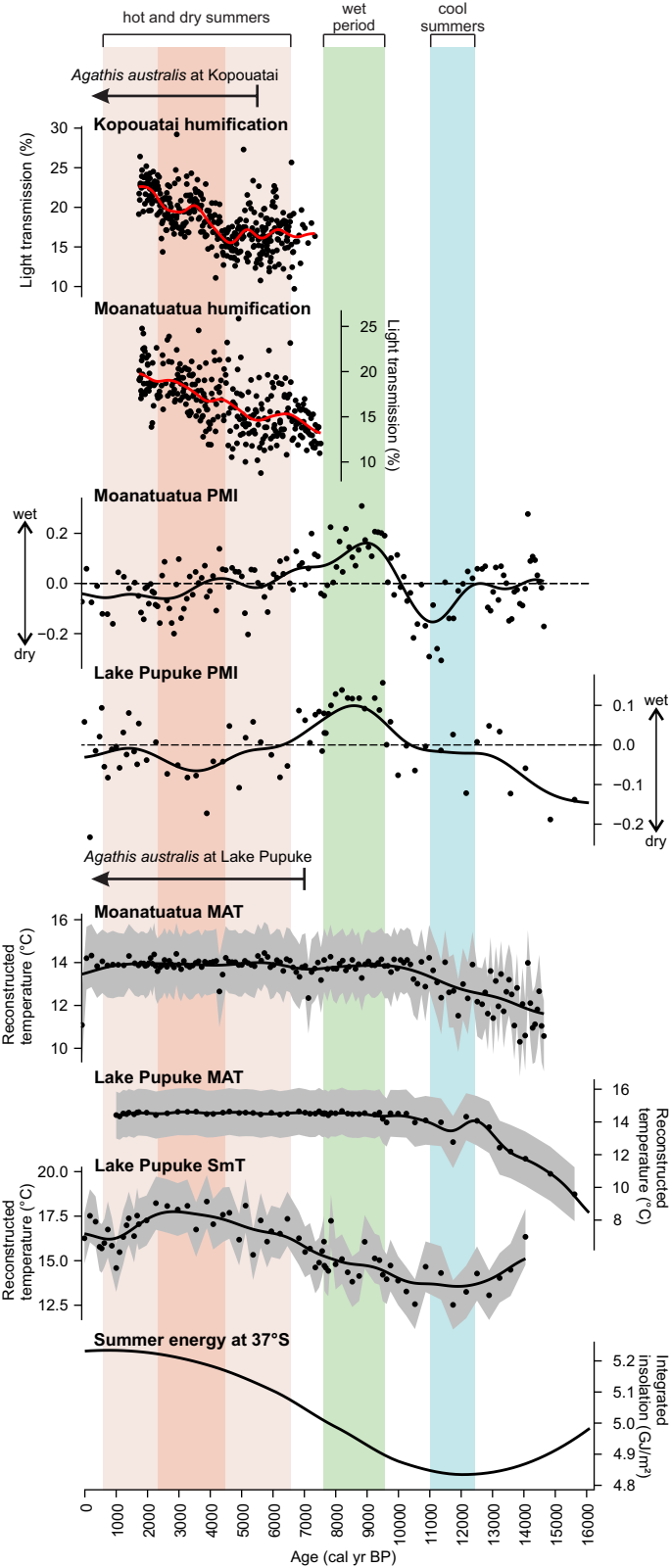


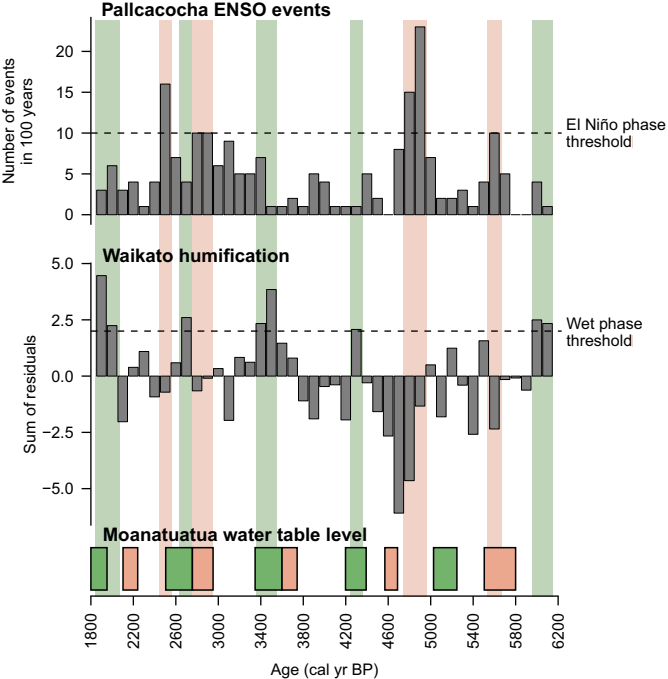
KEY

- Peat
- Sampling position for ¹⁴C date
- Lab code
- Visible tephra
- Cryptotephra









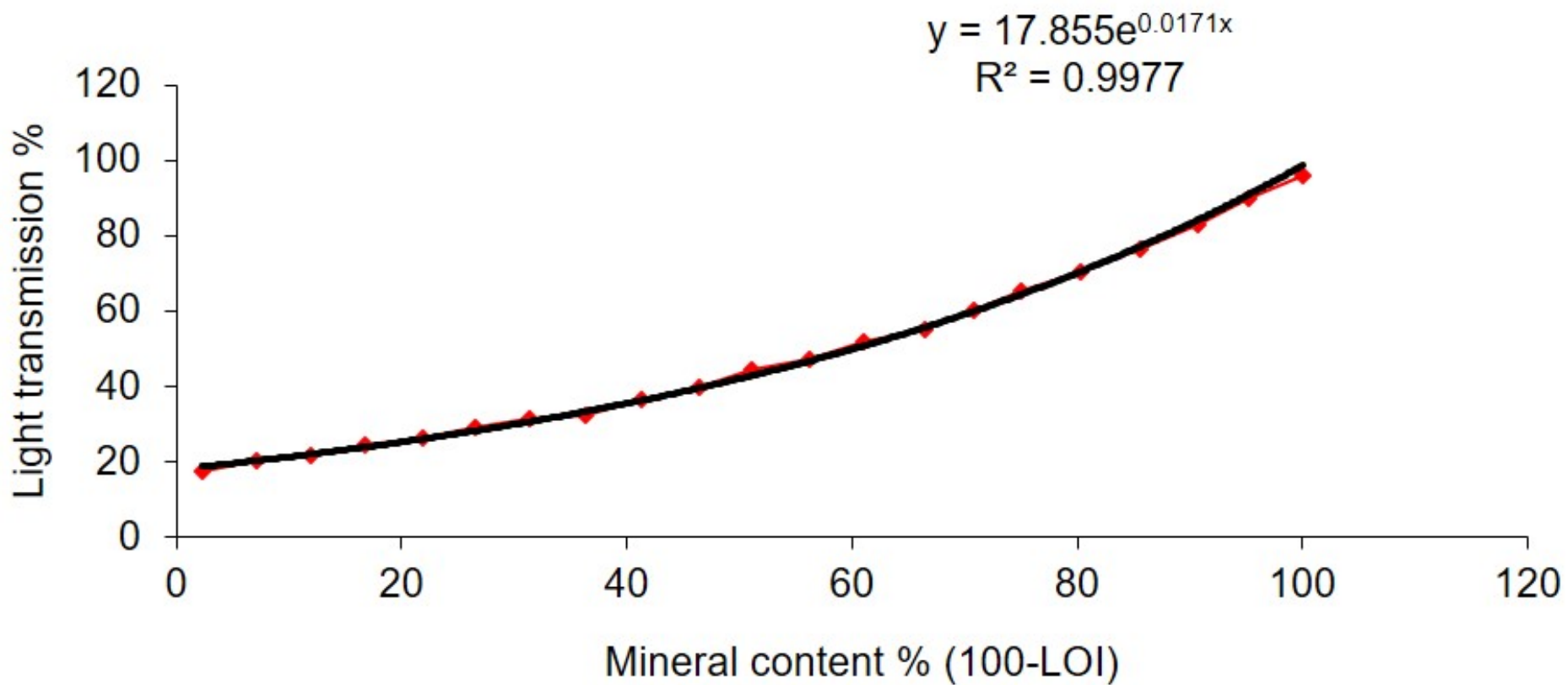
Legend:

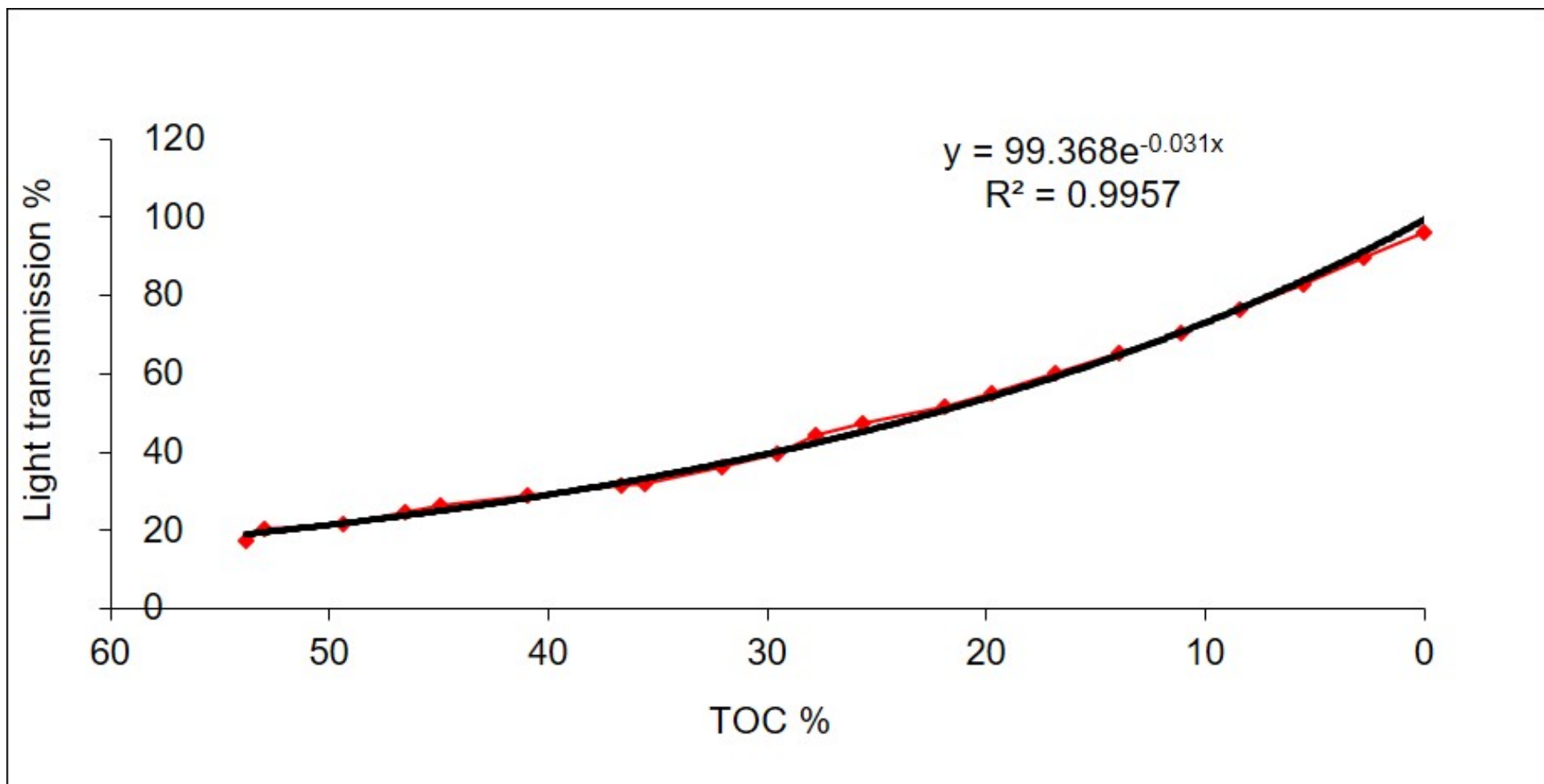
Extreme high

Extreme low

Wet phase in Waikato bogs

Warm El Niño phase





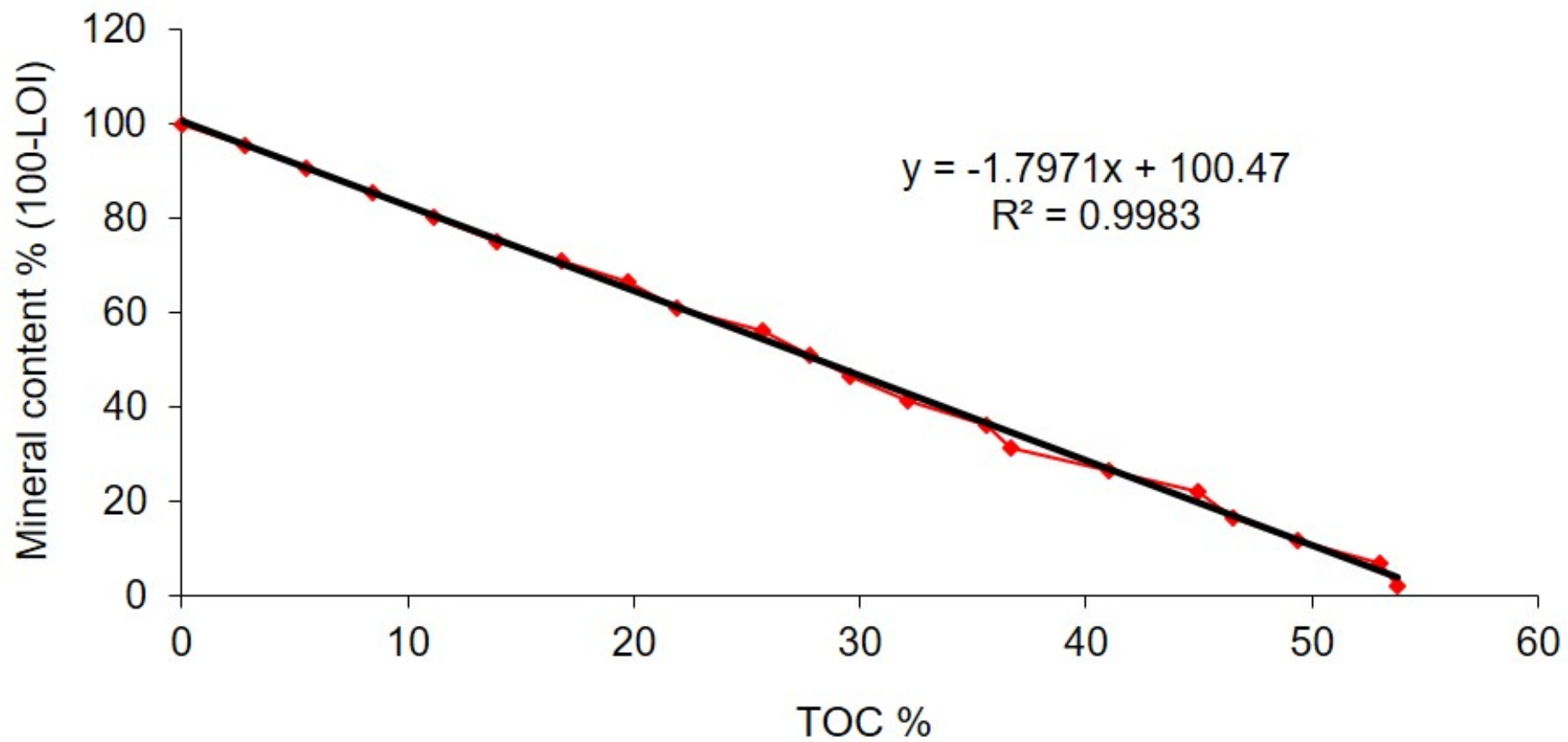


Table 1. Calendrical ages of visible tephras and cryptotephras in Kopuatai and Moanatuatua bogs

Core	Tephra ^{a, c}	Depth.min	Depth.max	Depth.ave	Age ($\pm 2\sigma$) cal yr BP	Basis of age ^d	Reference
K106	Taupo	281	282	281.5	1718 \pm 10	Dendro	Hogg et al. (2012)
	Whakaipo (ct)	375	375	375	2800 \pm 60	Tau bound	Lowe et al. (2013)
	?Unit Q (Stent) (ct) ^c	537	537	537	4322 \pm 112	Tau bound	Lowe et al. (2013)
	Unit K (ct)	546	546	546	5088 \pm 73	P sequen	Lowe et al. (2013)
	Whakatane ^b (ct)	563	563	563	5542 \pm 48	P sequen	Lowe et al. (2013)
	Tuhua	785	786	785.5	7027 \pm 170	Tau bound	Lowe et al. (2013)
	Mamaku	809	810	809.5	7992 \pm 58	P sequen	Lowe et al. (2013)
K108	Taupo	336	337	336.5	1718 \pm 10	Dendro	Hogg et al. (2012)
	Tuhua	737	738	737.5	7027 \pm 170	Tau bound	Lowe et al. (2013)
	Mamaku	778	779	778.5	7992 \pm 58	P sequen	Lowe et al. (2013)
	Rotoma	794	795	794.5	9472 \pm 40	P sequen	Lowe et al. (2013)
	Waiohau	874	875	874.5	14018 \pm 91	P sequen	Lowe et al. (2013)
K204	Kaharoa ^c	230	235	232.5	636 \pm 12	Dendro	Hogg et al. (2003)
	Taupo	370	371	370.5	1718 \pm 10	Dendro	Hogg et al. (2012)
	Tuhua	875	876	875.5	7027 \pm 170	Tau bound	Lowe et al. (2013)
M102	Taupo	50	51	50.5	1718 \pm 10	Dendro	Hogg et al. (2012)
	Whakaipo	102	103	102.5	2800 \pm 60	Tau bound	Lowe et al. (2013)
	Tuhua	307	308	307.5	7027 \pm 170	Tau bound	Lowe et al. (2013)
	Mamaku	336	337	336.5	7992 \pm 58	P sequen	Lowe et al. (2013)
M103	Taupo	159	160	159.5	1718 \pm 10	Dendro	Hogg et al. (2012)
	Whakaipo (ct)	210	210	210	2800 \pm 60	Tau bound	Lowe et al. (2013)
	Tuhua	473	475	474	7027 \pm 170	Tau bound	Lowe et al. (2013)

	Mamaku	489.5	490.5	490	7992 ± 58	P sequen	Lowe et al. (2013)
M206	Taupo	157	158	157.5	1718 ± 10	Dendro	Hogg et al. (2012)
	Tuhua	500	510	505	7027 ± 170	Tau bound	Lowe et al. (2013)
	Mamaku	537	538	537.5	7992 ± 58	P sequen	Lowe et al. (2013)

^a See Fig. 2; ct = cryptotephra. Depths in centimetres

^b Also contained Unit-K glass (Gehrels et al., 2006)

^c Not used in age modelling here.

^d Dendro = age based on dendrochronology and wiggle-matching

Tau bound = age modelled using Tau-boundary function of OxCal

P sequen = age modelled using P_sequence function of OxCal

^e Two uncorrelated Egmont-derived cryptotephtras, one aged c. 5.2 cal ka in K108 and one aged c. 7.4 cal ka in K204 (Fig. 2), were not used in age modelling.

Table 2 Electron microprobe analyses^a of glass shards from tephra/cryptotephra in Kopuatai bog

Tephra ^b	Kaharoa	Taupo (Y)			Whakaipo (V)	Stent (Q) (?)	Unit K	Unit K (5a) and Whakatane (5b)	
Core number	Hodder <i>et al.</i> (1991) ^c	Z106 (1a) ^f	Z108	Z204	Z106 (2) ^f	Z106 (3a) ^f	Z106 (4) ^f	Z106 (5a) ^f	Z106 (5b) ^f
Depth (m)	2.50-2.52	2.79-2.80	3.36-3.37	3.70-3.71	3.75-3.76	5.37-5.38	5.46-5.47	5.63-5.64	
SiO ₂	78.22 (0.31)	75.00 (0.35)	75.86 (0.72)	75.88 (0.83)	76.64 (0.25)	75.81 (0.57)	74.89 (0.76)	75.86 (0.20)	77.52 (0.73)
Al ₂ O ₃	12.49 (0.15)	13.45 (0.20)	13.21 (0.42)	13.40 (0.31)	12.77 (0.25)	13.33 (0.20)	13.01 (0.22)	13.32 (0.10)	12.57 (0.35)
TiO ₂	0.13 (0.04)	0.29 (0.06)	0.23 (0.06)	0.25 (0.06)	0.16 (0.03)	0.19 (0.03)	0.21 (0.05)	0.24 (0.05)	0.11 (0.03)
FeO ^c	0.76 (0.26)	2.02 (0.28)	1.82 (0.19)	1.75 (0.28)	1.59 (0.20)	1.79 (0.14)	1.64 (0.24)	1.66 (0.15)	0.90 (0.07)
MnO	na	0.12 (0.05)	0.10 (0.06)	0.08 (0.06)	0.13 (0.02)	0.09 (0.08)	0.09 (0.06)	0.10 (0.10)	0.05 (0.04)
MgO	0.09 (0.13)	0.28 (0.04)	0.24 (0.05)	0.26 (0.05)	0.13 (0.02)	0.18 (0.03)	0.19 (0.03)	0.19 (0.02)	0.10 (0.02)
CaO	0.55 (0.06)	1.49 (0.11)	1.42 (0.18)	1.42 (0.10)	1.02 (0.04)	1.30 (0.10)	1.29 (0.11)	1.25 (0.08)	0.69 (0.06)
Na ₂ O	3.42 (0.19)	4.37 (0.20)	4.07 (0.14)	3.99 (0.25)	4.28 (0.14)	4.08 (0.43)	4.20 (0.13)	4.25 (0.15)	3.90 (0.15)
K ₂ O	4.22 (0.43)	2.79 (0.13)	2.88 (0.32)	2.82 (0.11)	3.17 (0.14)	3.08 (0.20)	3.12 (0.21)	2.98 (0.11)	3.98 (0.14)
Cl	0.14 (0.03)	0.18 (0.05)	0.16 (0.03)	0.17 (0.05)	0.16 (0.06)	0.13 (0.03)	0.12 (0.03)	0.16 (0.04)	0.19 (0.05)
Water ^d	0.93 (0.68)	2.95 (1.00)	1.76 (1.62)	4.18 (2.93)	3.10 (1.82)	2.07 (1.43)	1.25 (0.89)	1.97 (0.16)	3.60 (0.98)
<i>n</i>	10	16 (+4) ^g	13 (+1) ^g	13	12	13 (+1) ^g	12	10	8

Table 2 cont

Tephra ^b	Egmont-derived (uncorr) ^h	Tuhua			Mamaku		Rotoma	Waiohau
Core number	Z204	Z106 (6) ^f	Z108	Z204	Z106	Z108	Z108	Z108
Depth (m)	8.42-8.43	7.84-7.85	7.37-7.38	8.75-8.76	8.09-8.10	7.78-7.79	7.94-7.95	8.74-8.75
SiO ₂	69.72 (0.82)	74.04 (0.59)	74.60 (0.40)	73.51 (0.98)	78.31 (0.30)	78.06 (0.30)	77.95 (0.07)	77.91 (0.51)
Al ₂ O ₃	15.75 (0.30)	9.53 (0.20)	9.58 (0.20)	9.92 (0.55)	12.28 (0.16)	12.35 (0.21)	12.41 (0.09)	12.62 (0.39)
TiO ₂	0.48 (0.06)	0.30 (0.06)	0.26 (0.04)	0.27 (0.08)	0.13 (0.04)	0.12 (0.05)	0.10 (0.00)	0.14 (0.06)
FeO ^c	1.94 (0.29)	5.68 (0.38)	5.44 (0.18)	5.57 (0.29)	0.81 (0.09)	0.88 (0.11)	0.74 (0.02)	0.84 (0.10)
MnO	0.10 (0.05)	0.15 (0.06)	0.15 (0.12)	0.19 (0.07)	0.07 (0.06)	0.06 (0.04)	0.08 (0.01)	0.11 (0.09)
MgO	0.48 (0.13)	0.01 (0.02)	0.02 (0.02)	0.03 (0.05)	0.11 (0.03)	0.11 (0.02)	0.07 (0.02)	0.12 (0.02)
CaO	1.34 (0.19)	0.24 (0.04)	0.24 (0.03)	0.28 (0.18)	0.71 (0.07)	0.72 (0.05)	0.52 (0.03)	0.77 (0.03)
Na ₂ O	4.62 (0.16)	5.61 (0.27)	5.26 (0.17)	5.64 (0.38)	3.78 (0.15)	3.93 (0.07)	4.03 (0.02)	3.97 (0.15)
K ₂ O	5.33 (0.12)	4.22 (0.12)	4.20 (0.14)	4.36 (0.14)	3.63 (0.14)	3.61 (0.14)	3.93 (0.06)	3.38 (0.10)
Cl	0.24 (0.04)	0.21 (0.02)	0.25 (0.04)	0.23 (0.03)	0.17 (0.04)	0.15 (0.04)	0.17 (0.03)	0.15 (0.04)
Water ^d	0.92 (1.26)	1.35 (1.22)	0.45 (0.51)	1.78 (1.16)	2.58 (1.24)	2.89 (1.95)	0.36 (0.33)	1.82 (1.29)
<i>n</i>	18	12 (+1) ^g	10	16	13	12	2	13

^aMeans and standard deviations (in parentheses) of *n* analyses (individual glass shards) normalised to 100% loss-free basis (wt%) (Lowe et al., 2017). Analyses by wavelength-dispersive Jeol JXA-733 Superprobe at the Analytical Facility, Victoria University of Wellington, were undertaken by Dr Kathryn Wilson using Smithsonian microbeam glass standards VG-568 and VG-99 (Jarosewich et al., 1980; Jarosewich,

2002) and other reference samples including KN18 (Froggatt, 1983) to correct for machine drift, defocussed beam diameter 20 µm, current 8 nA, and accelerating voltage 15 kV; Na analysed first, no peak search; analyses calculated from 11 x 2 s counts across the peak, curve integrated. na, not available.

^bTephra names from Froggatt and Lowe (1990); letters are equivalent volcanological units of Wilson (1993). Stent tephra (Unit Q) defined by Alloway *et al.* (1994).

^cTotal Fe expressed as FeO.

^dWater by difference from original analytical total.

^eFrom Hodder *et al.* (1991, p. 198) (core 22 of Newnham *et al.*, 1995).

^fAnalyses from Gehrels *et al.* (2006, p. 178) (numbers in parentheses in column headers refer to their analysis numbers).

^gValues in parentheses in this line refer to minor subpopulations of different glass composition (not reported here; see Gehrels *et al.*, 2006).

^hThis currently-uncorrelated Egmont-derived cryptotephra (c. 7.4 cal. ka) is possibly a correlative of Eg-7 of Lowe (1988) and likely to be a correlative with a unit of the lower part of *Tephra Sequence C* (c. 9.5-6.8 cal. ka) of Damaschke *et al.* (2017). The Egmont-derived cryptotephra at c. 5.7 m (c. 5.4 cal. ka) in core K108 (no glass analyses) is likely to be a correlative with a unit of the upper part of *Tephra Sequence C* (c. 6-4.3 cal. ka) of Damaschke *et al.* (2017).

Table 3 Electron microprobe analyses^a of glass shards from tephras^b in Moanatuatua bog

Tephra ^c	Taupo (Y)		Whakaipo (V)	Tuhua	Mamaku			
Core number	M103	M206	M102	M102	M102	M103	M203	M206
Depth (m)	1.59-1.60	1.57-1.58	1.02-1.03	3.07-3.08	3.36-3.37	4.90-4.91	3.45-3.46	5.37-5.38
SiO ₂	75.47 (0.27)	75.32 (0.69)	77.45 (0.46)	74.63 (0.42)	78.14 (0.46)	78.20 (0.17)	77.52 (0.20)	77.59 (0.37)
Al ₂ O ₃	13.43 (0.10)	13.50 (0.23)	12.40 (0.27)	9.98 (0.61)	12.57 (0.34)	12.36 (0.10)	12.57 (0.18)	12.62 (0.26)
TiO ₂	0.26 (0.04)	0.21 (0.09)	0.16 (0.06)	0.27 (0.04)	0.11 (0.05)	0.11 (0.02)	0.11 (0.04)	0.10 (0.03)
FeO ^d	1.94 (0.14)	1.81 (0.17)	1.45 (0.08)	5.40 (0.28)	0.82 (0.08)	0.85 (0.08)	0.88 (0.10)	0.92 (0.17)
MnO	0.12 (0.05)	0.12 (0.10)	0.09 (0.04)	0.14 (0.05)	0.08 (0.04)	0.08 (0.05)	0.06 (0.05)	0.09 (0.06)
MgO	0.27 (0.07)	0.26 (0.11)	0.14 (0.04)	0.02 (0.03)	0.11 (0.03)	0.10 (0.01)	0.14 (0.05)	0.13 (0.08)
CaO	1.49 (0.06)	1.40 (0.15)	0.98 (0.15)	0.23 (0.03)	0.71 (0.06)	0.72 (0.06)	0.75 (0.05)	0.73 (0.10)
Na ₂ O	4.08 (0.18)	4.32 (0.30)	4.05 (0.22)	4.92 (0.65)	3.70 (0.26)	3.82 (0.15)	3.99 (0.15)	4.00 (0.19)
K ₂ O	2.77 (0.07)	2.90 (0.15)	3.13 (0.10)	4.16 (0.06)	3.59 (0.11)	3.60 (0.12)	3.81 (0.18)	3.65 (0.18)
Cl	0.17 (0.04)	0.15 (0.03)	0.15 (0.03)	0.24 (0.03)	0.17 (0.04)	0.17 (0.04)	0.16 (0.02)	0.16 (0.03)
Water ^e	0.77 (0.70)	1.88 (1.14)	1.08 (0.48)	0.81 (0.72)	1.46 (1.28)	1.47 (0.94)	1.44 (1.53)	2.25 (1.48)
<i>n</i>	9	16	4	11	11	7	10	16

^aMeans and standard deviations (in parentheses) of *n* analyses (individual glass shards) normalised to 100% loss-free basis (wt%) (Lowe et al., 2017). Analyses were undertaken as described in Table 2.

^bSee also analyses of glass shards of older Waiohau and Rotorua tephras from the base of Moanatuatua bog presented by Jara et al. (2017, their Table S1).

^cTephra names from Froggatt and Lowe (1990); letters are equivalent volcanological units of Wilson (1993).

^dTotal Fe as FeO.

^eWater by difference from original analytical total.

Table 4. AMS and bulk radiocarbon ages from Kopouatai and Moanatuatua bogs and age calibrations.

Core	Lab number ^a	Ave. depth and sample width (cm)	¹⁴ C age ^b ± 1 σ	δ ¹³ C	Unmodelled			Modelled		A _{index}	
					95% max	95% min	Mean	95% max	95% min		Mean
K106	AA-54136	341.5 (1.8)	2347 ± 38	-26.4	2436	2161	2310	2455	2188	2332	114.6
	AA-54137	390.0 (1.0)	2962 ± 38	-29.1	3209	2930	3064	3165	2925	3036	101.6
	AA-54138	445.0 (1.2)	3618 ± 39	-29.8	3984	3719	3873	3975	3721	3855	101.5
	AA-54139	498.8 (1.1)	4116 ± 41	-29.9	4812	4425	4597	4695	4420	4536	107.4
	SUERC-1481	556.2 (1.1)	4433 ± 37	-30.2	5267	4851	4976	5270	4952	5100	54.8
	SUERC-1482	609.5 (1.0)	4925 ± 34	-30.1	5715	5488	5621	5714	5490	5621	103.1
	SUERC-1483	664.5 (2.3)	5039 ± 39	-30.0	5892	5613	5745	5893	5613	5745	
	SUERC-1517	736.6 (1.0)	6017 ± 34	-30.9	6930	6679	6810	6968	6732	6853	88.0
K108	AA-54140	379.7 (1.1)	2404 ± 40	-29.8	2694	2310	2426	2686	2308	2413	104.5
	AA-54141	425.7 (1.0)	2832 ± 37	-29.7	2995	2782	2890	3000	2781	2894	100.7
	AA-54142	464.3 (1.5)	3352 ± 38	-30.2	3679	3446	3537	3681	3446	3537	100.5
	AA-54143	512.7 (1.1)	4145 ± 40	n/a	4821	4447	4642	4817	4445	4628	100.4
	AA-54144	559.2 (1.1)	4514 ± 41	-28.5	5303	4894	5131	5303	4963	5138	102.0
	SUERC-1484	603.1 (2.0)	4999 ± 37	-29.0	5863	5596	5690	5874	5596	5692	100.4
	SUERC-1485	648.7 (2.1)	5707 ± 33	-28.9	6551	6320	6446	6550	6320	6444	100.9
	SUERC-1486	689.0 (2.1)	6101 ± 30	-27.3	7005	6791	6911	7008	6790	6911	100.9
K204	SUERC-1496	417.5 (1.0)	2165 ± 28	-28.6	2299	2010	2116	2299	2017	2129	104.6
	SUERC-1497	462.5 (1.0)	2543 ± 28	-28.8	2741	2458	2591	2736	2497	2622	102.8
	SUERC-1501	506.5 (1.0)	3056 ± 28	-30.7	3340	3076	3208	3331	3076	3199	106.1
	SUERC-1502	551.5 (1.0)	3484 ± 29	-29.3	3829	3610	3710	3833	3629	3727	97.9
	SUERC-1503	595.5 (1.0)	3992 ± 32	-30.7	4520	4256	4398	4514	4250	4376	97.6
	SUERC-1504	640.5 (1.0)	4344 ± 34	-30.2	5026	4825	4880	5033	4827	4902	84.0
	SUERC-1505	684.5 (1.0)	5084 ± 33	n/a	5903	5663	5800	5888	5652	5745	80.7
	SUERC-1507	730.0 (2.0)	5429 ± 31	n/a	6286	6017	6188	6288	6029	6203	108.2
	Wk-11111	777.0 (2.0)	5983 ± 185	-29.1	7252	6399	6798	6948	6495	6721	122.9
	Wk-11110	827.0 (2.0)	6526 ± 174	-30.2	7681	6992	7369	7430	7049	7248	92.0
Wk-11109	845.0 (2.0)	6571 ± 151	-28.7	7693	7030	7420	7553	7257	7399	120.3	
Wk-11108	929.0 (2.0)	7624 ± 165	-30.1	8857	8014	8401	8549	8024	8295	104.0	

Core	Lab no.	Ave. depth and sample width (cm)	¹⁴ C age ± 1 σ	δ ¹³ C	Unmodelled			Modelled			A _{index}
					95% max	95% min	Mean	95% max	95% min	Mean	
M102	SUERC-2520	79.5 (1.0)	1962 ± 24	n/a	1928	1755	1867	1928	1755	1867	
	SUERC-1508	109.0 (2.0)	2825 ± 28	-28.0	2960	2785	2880	2958	2792	2882	105.3
	SUERC-1511	138.5 (1.0)	3434 ± 29	-28.2	3816	3515	3639	3717	3515	3628	103.1
	SUERC-1512	164.0 (2.0)	3789 ± 29	n/a	4231	3984	4099	4239	3995	4131	98.4
	SUERC-1513	192.5 (1.0)	4474 ± 29	-27.8	5279	4872	5057	5254	4866	5000	106.3
	SUERC-1514	221.5 (1.0)	4340 ± 27	-28.2	4961	4827	4870	4961	4827	4870	
	SUERC-1515	248.5 (1.0)	5574 ± 29	-28.5	6400	6283	6336	6401	6281	6332	101.7
	SUERC-1516	277.5 (1.0)	6106 ± 36	n/a	7151	6788	6921	7141	6795	6927	106.4
	Wk-11106	348.5 (3.0)	6071 ± 127	-28.3							
M103	Wk-11112	533.5 (3.0)	9454 ± 206	-28.6							
	AA-54133	195.6 (1.2)	2408 ± 38	-28.5	2690	2315	2429	2496	2348	2435	93.9
	SUERC-1473	237.6 (1.2)	3111 ± 28	-29.1	3365	3180	3279	3341	3179	3257	100.3
	SUERC-1474	267.9 (1.4)	3574 ± 32	-28.2	3914	3695	3804	3885	3715	3794	109.4
	SUERC-1475	302.0 (1.0)	3801 ± 33	-27.8	4240	3985	4119	4240	3985	4119	
	SUERC-1476	331.8 (2.3)	4386 ± 35	-29.0	5038	4839	4922	5026	4845	4923	106.2
	AA-54134	366.6 (1.2)	4817 ± 43	-28.4	5600	5327	5499	5603	5472	5548	107.8
	SUERC-1480	403.1 (1.1)	5466 ± 40	-29.1	6306	6025	6222	6301	6189	6251	113.2
AA-54135	440.0 (1.1)	6240 ± 46	-28.2	7249	6969	7097	7119	6927	7015	84.9	

M206	SUERC-1490	196.5 (1.0)	2139 ± 24	-29.0	2149	2008	2075	2300	2009	2122	80.0
	SUERC-1491	234.5 (1.0)	2899 ± 28	-28.5	3075	2865	2973	3058	2863	2948	101.1
	SUERC-1492	271.5 (1.0)	3256 ± 26	-29.4	3555	3364	3433	3548	3364	3431	103.8
	SUERC-1493	308.5 (1.0)	3609 ± 30	-28.3	3974	3724	3860	4065	3733	3895	96.5
	SUERC-1495	346.5 (1.0)	4294 ± 32	-29.0	4875	4630	4800	4873	4629	4786	91.3
	SUERC-1518	383.5 (1.0)	4755 ± 25	-29.3	5581	5323	5441	5580	5323	5438	99.3
	SUERC-1521	422.0 (2.0)	5381 ± 31	-28.1	6268	5997	6115	6269	6000	6124	100.9
	SUERC-1522	458.5 (1.0)	6079 ± 37	-29.0	6999	6753	6882	6980	6751	6868	102.2
	Wk-11107	542.5 (1.0)	5952 ± 152	-28.3	7157	6410	6755	7157	6411	6755	

^aAA- and SUERC- samples were processed as two separate batches at the NERC Radiocarbon Laboratory (East Kilbride, UK), while Wk- samples were processed at the Waikato Radiocarbon Dating Laboratory (Hamilton, New Zealand). AA- and SUERC- samples were measured using AMS on above-ground plant macrofossils, mainly *Leptospermum scoparium* and *Epacris pauciflora* leaves. Where these were absent, *Epacris* and cf. *Empodisma* seeds and *Gleichenia dicarpa* fronds were used. Wk- samples comprised bulk peat. Age-depth models were developed using OxCal v4.3.2 (Bronk Ramsey, 2009) and the SHCal13 atmospheric curve (Hogg et al., 2013). Each core was modelled with P_Sequence (Bronk Ramsey, 2008) and tephra layers were cross-referenced between cores. Outliers are denoted by missing A_{index} values, “n/a” indicates no result because of insufficient sample, and Wk-11106 and Wk-11112 were sampled from separate cores adjacent to M102. Although not used in this study, these last two dates are included here for completeness.

^bConventional radiocarbon ages in ^{14}C year BP \pm 1 standard deviation (σ)

Table 5. Pearson correlation coefficients (r) and p-values for correlation between the 100-year bins of humification records for the three Kopouatai and Moanatuatua cores

	K106R	K108R
K108R	0.009 (p=0.951)	
K204R	0.329 (p=0.029)*	0.313 (p=0.038)*

	M102R	M103R
M103R	0.284 (p=0.043)*	
M206R	0.130 (p=0.365)	0.085 (p=0.552)

* Denotes a significant correlation at the 95% certainty level.